Article

Immunity

Human Secretory IgM Emerges from Plasma Cells Clonally Related to Gut Memory B Cells and Targets Highly Diverse Commensals

Graphical Abstract

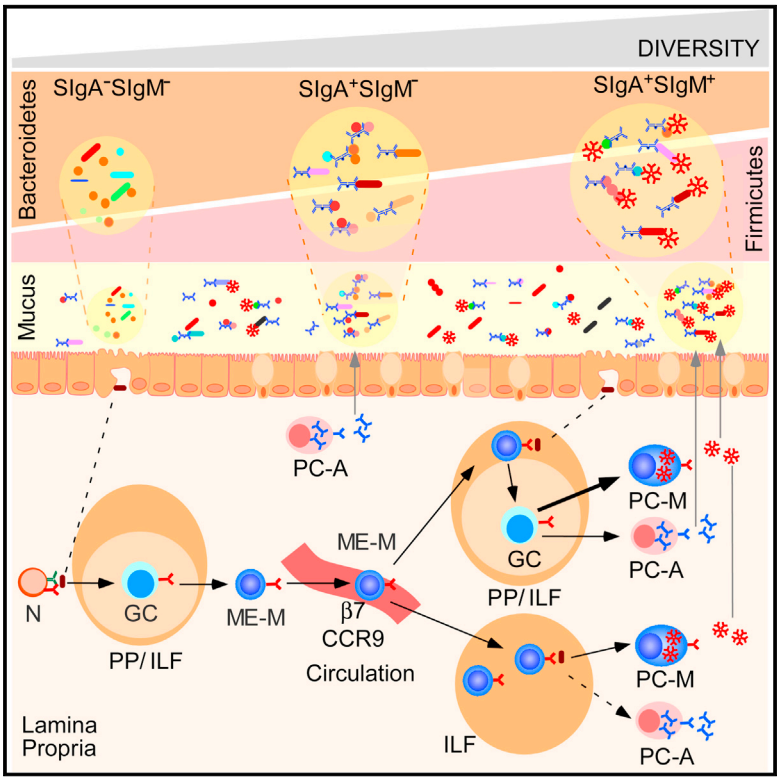

Highlights

- IgM⁺ PCs generating SIgM are relatively abundant in human but not mouse gut
- IgM⁺ PCs clonally relate to a large gut repertoire of memory IgM⁺ B cells
- Gut memory IgM⁺ B cells express a tissue-specific signature and can switch to IgA
- Human but not mouse SIgM binds a highly diverse microbiota dually coated by SIgA

Authors

Giuliana Magri, Laura Comerma, Marc Pybus, ..., Elena Mercade, Saurabh Mehandru, Andrea Cerutti

Correspondence

gmagri@imim.es (G.M.), acerutti@imim.es (A.C.)

In Brief

Magri et al. found that the human gut includes a large memory IgM⁺ B cell repertoire clonally related to plasma cells mounting SIgM responses against mucus-embedded commensals co-targeted by SIgA. Dually coated bacteria are detected in humans but not mice and show increased diversity and richness compared to SIgA-only-coated or uncoated bacteria.

Magri et al., 2017, Immunity *47*, 118–134
July 18, 2017
http://dx.doi.org/10.1016/j.immuni.2017.06.013

CellPress

Immunity
Article

Human Secretory IgM Emerges from Plasma Cells Clonally Related to Gut Memory B Cells and Targets Highly Diverse Commensals

Giuliana Magri,[1,11,*] Laura Comerma,[1,11] Marc Pybus,[1] Jordi Sintes,[1] David Lligé,[1] Daniel Segura-Garzón,[1] Sabrina Bascones,[1] Ada Yeste,[1] Emilie K. Grasset,[2,3] Cindy Gutzeit,[2] Mathieu Uzzan,[2] Meera Ramanujam,[4] Menno C. van Zelm,[5] Raquel Albero-González,[6] Ivonne Vazquez,[6] Mar Iglesias,[6,7] Sergi Serrano,[6,7] Lucía Márquez,[8] Elena Mercade,[9] Saurabh Mehandru,[2] and Andrea Cerutti[1,2,10,12,*]

[1]Program for Inflammatory and Cardiovascular Disorders, Institut Hospital del Mar d'Investigacions Mèdiques (IMIM), Barcelona 08003, Spain
[2]Department of Medicine, Immunology Institute, Icahn School of Medicine at Mount Sinai, New York, NY 10029, USA
[3]Department of Medicine, Center for Molecular Medicine, Karolinska University Hospital, Karolinska Institutet, Stockholm 171 76, Sweden
[4]Immunology and Respiratory Disease Research, Boehringer Ingelheim Pharmaceuticals, Ridgefield, CT 06877, USA
[5]Department of Immunology and Pathology, Monash University and Alfred Hospital, Melbourne, VIC 3004, Australia
[6]Pathology Department, Hospital del Mar, Barcelona 08003, Spain
[7]Universitat Autònoma de Barcelona, Barcelona 08003, Spain
[8]Department of Gastroenterology, Hospital del Mar, Barcelona 08003, Spain
[9]Department of Biology, Health and Environment, University of Barcelona, Barcelona 08028, Spain
[10]Catalan Institute for Research and Advanced Studies (ICREA), Barcelona 08003, Spain
[11]These authors contributed equally
[12]Lead Contact
*Correspondence: gmagri@imim.es (G.M.), acerutti@imim.es (A.C.)
http://dx.doi.org/10.1016/j.immuni.2017.06.013

SUMMARY

Secretory immunoglobulin A (SIgA) enhances host-microbiota symbiosis, whereas SIgM remains poorly understood. We found that gut IgM$^+$ plasma cells (PCs) were more abundant in humans than mice and clonally related to a large repertoire of memory IgM$^+$ B cells disseminated throughout the intestine but rare in systemic lymphoid organs. In addition to sharing a gut-specific gene signature with memory IgA$^+$ B cells, memory IgM$^+$ B cells were related to some IgA$^+$ clonotypes and switched to IgA in response to T cell-independent or T cell-dependent signals. These signals induced abundant IgM which, together with SIgM from clonally affiliated PCs, recognized mucus-embedded commensals. Bacteria recognized by human SIgM were dually coated by SIgA and showed increased richness and diversity compared to IgA-only-coated or uncoated bacteria. Thus, SIgM may emerge from pre-existing memory rather than newly activated naive IgM$^+$ B cells and could help SIgA to anchor highly diverse commensal communities to mucus.

INTRODUCTION

Complex commensal communities generally referred to as microbiota colonize the gut mucosa soon after birth and have a broad impact on host metabolism, immune system development, and gut homeostasis (Kamada et al., 2013). A central element of gut homeostasis is secretory immunoglobulin A (SIgA), an antibody that promotes symbiotic host-microbiota interactions by binding commensals inhabiting the small intestine and, to a lesser extent, the large intestine (Bunker et al., 2015; Kawamoto et al., 2014).

SIgA responses to commensals mostly initiate at gut follicular sites of antigen entry, including Peyer's patches. At these sites, sampling of commensals by microfold cells, macrophages, and dendritic cells promotes a sustained germinal center (GC) reaction involving cognate interaction of B cells with T cells, followed by B cell induction of IgM-to-IgA class switching and affinity maturation through class switch recombination (CSR) and somatic hypermutation (SHM), respectively (Kawamoto et al., 2014). High-affinity and IgA-expressing B cells emerging from GCs upregulate gut-homing receptors and progressively differentiate into IgA-secreting plasma cells (PC-As), which home to the gut lamina propria (LP) (Macpherson et al., 2008). These PC-As release polymeric IgA, which translocates across epithelial cells to generate intraluminal SIgA that coats mucus-embedded commensals (Kubinak and Round, 2016).

The T cell-dependent (TD) pathway is complemented by a T cell-independent (TI) pathway entailing activation of follicular and possibly extrafollicular B cells by various cells of the innate immune system (Tsuji et al., 2008). Complementary TD and TI responses generate circulating IgA class-switched memory (ME-A) B cells and cooperatively shape the architecture of the microbiota during the development of an individual (Planer et al., 2016). However, the TD pathway may become predominant over time due to continuous accumulation of ME-A B cells (Lindner et al., 2012, 2015).

ME-A B cells emerge from gut inductive sites along with PC-As and continuously diversify their B cell receptor repertoire via a microbiota-stimulated adaptation process involving induction

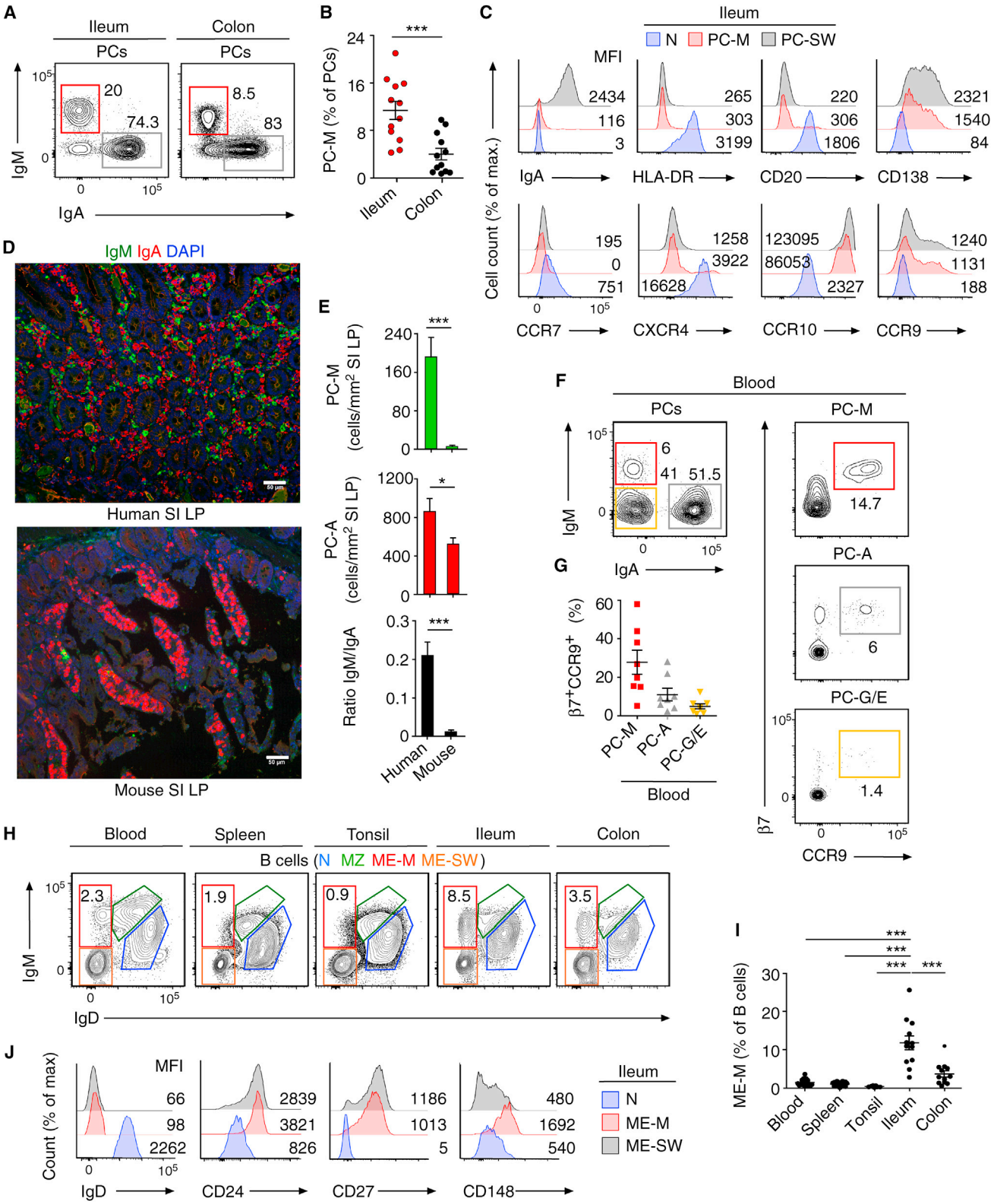

Figure 1. Human PC-Ms Accumulate in the Gut together with ME-M B Cells and Include a Circulating Counterpart Expressing Gut-Homing Receptors

(A) Flow cytometry (FCM) of IgM and IgA on CD19^{+}CD38^{hi}CD10^{-} PCs from human ileum and colon.

(B) Frequency of PC-Ms among total PCs, assessed by FCM.

(legend continued on next page)

of SHM and PC-A differentiation in pre-existing GCs (Lindner et al., 2012).

In addition to PC-As, the gut mucosa contains IgM-secreting PCs (PC-Ms) that release SIgM into the lumen through the polymeric Ig receptor (pIgR) (Macpherson et al., 2008). In mice, SIgM production increases upon induction of colonic damage to prevent lethal dissemination of commensals (Kirkland et al., 2012). However, little else is known about the ontogeny, regulation, and function of SIgM, particularly in humans. A better understanding of this mucosal antibody may further elucidate host-microbiota interactions in health and disease states. Indeed, primary antibody deficiency patients selectively lacking SIgA rarely develop inflammatory bowel disease, which is instead more common and very severe in patients lacking both SIgM and SIgA (Agarwal and Mayer, 2009).

We found that human PC-Ms coexisted with a large but previously unrecognized repertoire of gut-specific memory IgM$^+$ (ME-M) B cells that were clonally related to PC-Ms as well as some ME-A B cells and PC-As. In addition to inducing IgM-to-IgA CSR, ME-M cells exposed to TD or TI signals secreted copious IgM that targeted mucus-embedded commensals, similar to SIgM from PC-Ms. Unlike its murine counterpart, human SIgM recognized bacteria dually coated by SIgA that were characterized by increased diversity compared to SIgA-only-coated or uncoated bacteria. Thus, SIgM may emerge from pre-existing ME-M B cells rather than newly activated naive B cells and could help SIgA to anchor highly diverse microbial communities to gut mucus.

RESULTS

Gut PC-Ms Are More Abundant in Humans than Mice

Gut PC-As have been extensively studied, but little is known about gut PC-Ms, which account for about 10%–20% of all gut PCs in humans (Macpherson et al., 2008). Flow cytometry identified PC-Ms in addition to PC-As in histologically normal resected tissues from terminal ileum and proximal colon samples of individuals undergoing right hemicolectomy due to malignancy, polyps, or angiodysplasia (Figures 1A and S1A). PC-Ms were consistently more abundant in the ileum compared to the colon and expressed a phenotype similar to that of class-switched PCs, which comprised mostly PC-As (Figures 1A–1C and S1B).

Compared to human gut naive B cells, PC-Ms showed increased expression of CD138, CCR10, and/or CCR9. Upregulation of these PC-associated molecules was coupled with downregulation of HLA-DR, CD20, and the follicle-associated chemokine receptors CCR7 and CXCR4. Notwithstanding their resemblance to PC-Ms, class-switched PCs expressed more CD138, which could reflect a more advanced maturation stage (Figure 1C and S1B; Nutt et al., 2015).

Quantitative real-time PCRs (qRT-PCRs) further determined that, compared to human intestinal naive B cells, PC-Ms contained more transcripts for BLIMP-1 and IRF4 (Figure S1C), two transcription factors required for PC differentiation (Nutt et al., 2015). In addition, PC-Ms contained more transcripts for BCL-2 (Figure S1C), an anti-apoptotic protein that may sustain human PC survival in the intestine (Nair et al., 2016). Of note, immunofluorescence analysis followed by tissue-based cell counting demonstrated that, compared to the human ileum LP, the small intestinal LP from wild-type C57BL/6 mice featured fewer PC-Ms accumulating intracellular IgM and a lower PC-M/PC-A ratio (Figures 1D and 1E). Flow cytometry confirmed that the frequency of PC-Ms was negligible compared to that of PC-As in the mouse small and large intestines (Figures S1D and S1E).

Given that PC-As colonize the small intestinal LP from the circulation through a mechanism involving $\alpha4\beta7$ and CCR9 gut-homing receptors (Macpherson et al., 2008), we further verified whether circulating PC-Ms expressed gut-homing properties. Compared to PC-As, a larger fraction of circulating PC-Ms co-expressed $\beta7$ and CCR9, whereas PC-G/Es showed little or no $\beta7$ and CCR9 (Figures 1F and 1G). Thus, PC-Ms are relatively abundant in the human but not mouse small intestine, resemble gut PC-As, and include a circulating fraction expressing gut-homing receptors.

Gut PC-Ms Coexist with a Large Repertoire of ME-M B Cells

Considering that gut PC-As emerge from ME-A B cells diversifying at gut inductive sites (Lindner et al., 2015), we hypothesized that PC-Ms coexisted with ME-M B cells in the human gut and followed published gating strategies and comparable isolation procedures to segregate IgM$^+$IgD$^-$CD27$^+$CD38$^-$ ME-M B cells from IgM$^+$IgD^{hi}CD27$^-$CD38$^-$ naive, IgM$^+$IgD^{lo}CD27$^+$CD38$^-$ marginal zone (MZ), and IgM$^-$IgD$^-$CD27$^+$CD38$^-$ class-switched memory (ME-SW) B cells (Berkowska et al., 2011; Descatoire et al., 2014). Of note, MZ B cells are heterogeneous due to progressive recruitment into GC responses that induce classical memory traits over time, including antigen-driven selection (Aranburu et al., 2017; Descatoire et al., 2014; Klein et al., 1998; Seifert et al., 2015). Nonetheless, MZ B cells exhibit

(C) FCM of selected surface molecules on naive (N) B cells, PC-Ms, and switched PCs (PC-SW) from human ileum. Numbers indicate mean fluorescence intensity (MFI).

(D) Immunofluorescence analysis (IFA) of IgM (green), IgA (red), and DNA (blue) in human ileum and mouse small intestine (SI) lamina propria (LP). Original magnification, 20×. Scale bars, 50 μm.

(E) Number of PC-Ms (top), PC-As (center) per mm^2 of LP, and PC-M/PC-A ratio (bottom) from human or mouse SI assessed following tissue IFA. Data summarize six different tissue samples where at least four high-power microscopic fields were analyzed.

(F and G) Representative FCM (F) and frequency (G) of $\beta7^+$CCR9$^+$ cells in human circulating PC-Ms, PC-As, and PC-G/Es.

(H) Representative FCM showing IgM versus IgD staining on CD19$^+$CD38$^-$CD10$^-$ B cells from different human tissues.

(I) Frequency of ME-M B cells from tissues shown in (H).

(J) FCM of IgD, CD24, CD27, and CD148 on naive, ME-M, and ME-SW B cells from ileum.

Data show one representative result (A, F, H) of 12 (B), 8 (G), or 52 (I) experiments or are from one experiment of at least 3 with similar results (C, D, J). Results are presented as mean ± SEM; two-tailed unpaired Student's t test (B and E) and one-way ANOVA with Tukey's post hoc test (I). *$p < 0.05$, **$p < 0.01$, ***$p < 0.001$. See also Figure S1.

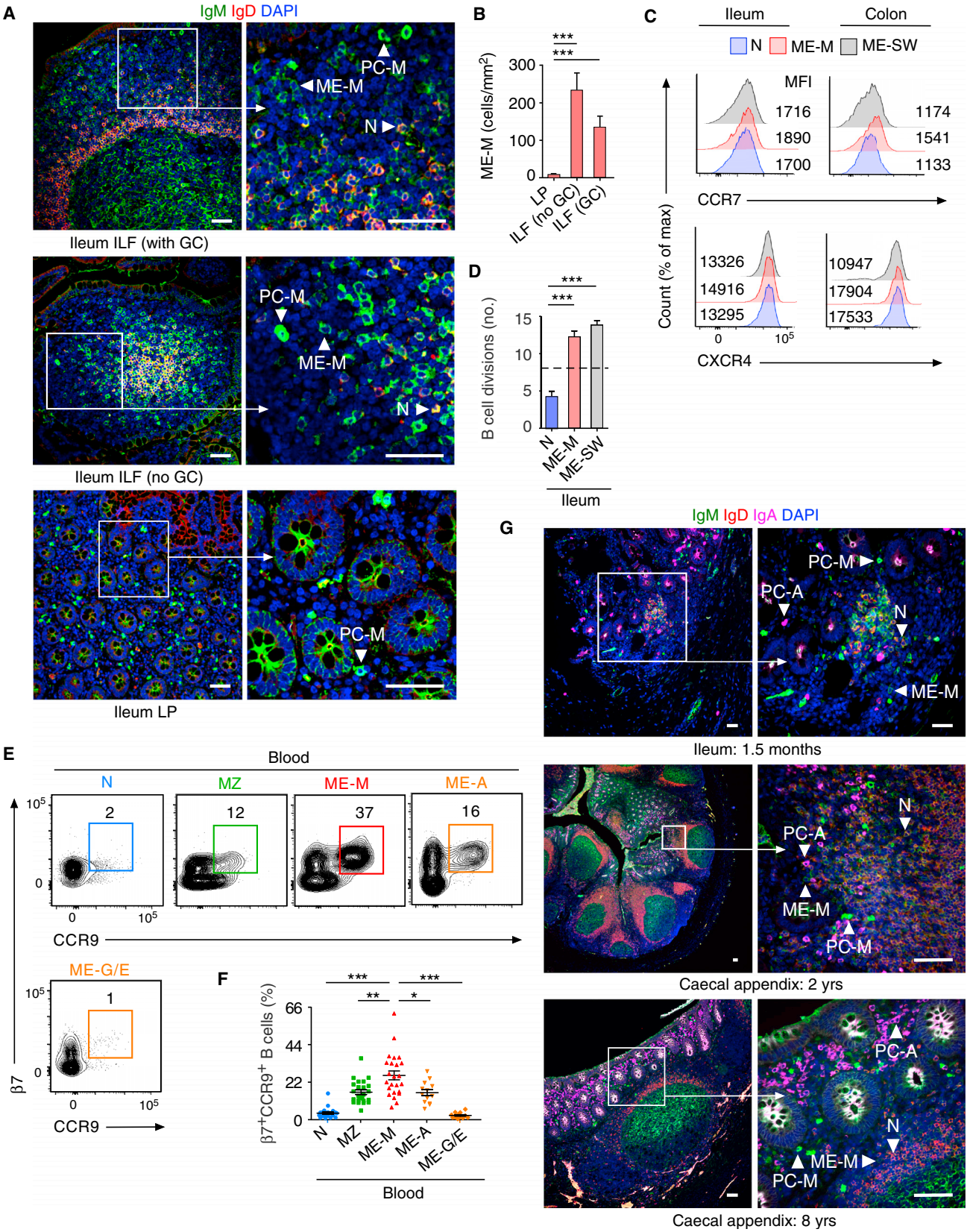

(legend on next page)

some properties that make them different from ME-M B cells, including NOTCH-dependent but GC-independent ontogeny in addition to IgD^{lo} phenotype (Aranburu et al., 2017; Berkowska et al., 2011; Descatoire et al., 2014). ME-M B cells were abundant in ileum and colon but rare in blood, spleen, and tonsil (Figures 1H and 1I). Consistent with the prevailing localization of PC-Ms in the ileum, ME-M B cells were enriched in the ileum compared to the colon and showed a phenotype similar to that of ileal ME-SW B cells and splenic MZ B cells, including increased expression of the co-stimulatory molecules CD24, CD27, and CD148 compared to naive B cells (Figures 1H–1J and S1F).

Next, we dissected the intestinal geography of ME-M B cells by tissue immunofluorescence. Tissue-based cell counting revealed that ME-M B cells expressing surface IgM but not IgD were rare in the gut LP and comparably abundant in ILFs with or without GCs (Figures 2A and 2B). Consistently, gut ME-M B cells expressed follicle-retaining CCR7 and CXCR4 receptors as much as gut naive and ME-SW B cells (Figure 2C). However, kappa-deleting recombination excision circle assays detected molecular fingerprints of GC proliferation (van Zelm et al., 2007) in gut ME-M and ME-SW but not naive B cells (Figure 2D).

Given that ME-A B cells upregulate $\alpha4\beta7$ and CCR9 gut-homing receptors as they recirculate from gut follicular inductive sites to the gut LP (Macpherson et al., 2008; Nair et al., 2016), we further determined $\beta7$ and CCR9 expression by circulating ME-M B cells. Compared to circulating ME-A B cells and MZ B cells, a larger fraction of circulating ME-M B cells co-expressed $\beta7$ and CCR9, whereas naive B cells and ME-G/E B cells showed little or no $\beta7$ and CCR9 co-expression (Figures 2E and 2F).

We then ascertained whether the gut mucosa generated ME-M B cells at an early age. Tissue immunofluorescence analysis identified human intestinal ME-M B cells together with PC-Ms and PC-As as early as 1.5 months of age (Figure 2G). Tissue-based cell counting and flow cytometry indicated that ME-M B cells remained stable over time, whereas PC-Ms increased through the first ten years of life (Figures S1G and S1H). Thus, human gut PC-Ms co-exist with a large and stable repertoire of ME-M B cells that emerge early in life, predominantly inhabit gut follicles, and include a circulating fraction expressing gut-homing receptors.

Gut ME-M B Cells Express a Gene Signature Reflecting Antigen Experience

Human intestinal ME-M B cells were further characterized through transcriptomics. These studies were preceded by a morphological analysis that confirmed the specificity of our sorting procedures (Figure 3A).

The global gene expression profile of ME-M B cells was elucidated through cross-comparative strategies involving memory B cell subsets from gut or spleen, including splenic MZ B cells. In this approach, each subset was compared to tissue-specific naive B cells. Supervised hierarchical clustering and robust multi-array average expression analysis indicated that ME-M B cells expressed a transcriptome distinct from that of naive B cells, but similar to that of ME-SW B cells, irrespective of the tissue of origin (Figures 3B and S2A). Venn diagrams further determined that gut ME-M B cells expressed a common memory B cell signature entailing 215 transcripts, which were also differentially expressed by gut ME-SW B cells as well as splenic ME-SW and MZ B cells (Figure S2B). This common memory B cell gene signature included increased expression of TACI (*TNFRSF13B*) along with decreased expression of IgD (*IGHD*), CD72, and the transcriptional suppressors of PC differentiation FOXO1, BTLA, and BACH2 (Figures S2C and S2D; Kurosaki et al., 2015; Nutt et al., 2015). Thus, human gut ME-M B cells express a common memory B cell gene signature reflecting increased propensity to undergo activation, proliferation, and PC differentiation.

Gut ME-M B Cells Express a Tissue-Specific Gene Signature

As shown by unsupervised hierarchical gene clustering and principal component analysis, gut ME-M and ME-SW B cells also expressed a tissue-specific signature. Indeed, these B cells clustered together but away from splenic ME-SW and MZ B cells, whereas naive B cells grouped together independently of their tissue of origin (Figures 3B, S2E, and S2F). Pairwise correlations confirmed that gut ME-M B cells were more robustly affiliated to gut ME-SW B cells than to splenic MZ B cells (Figure 3C). Accordingly, volcano plot, Venn diagram, and heatmap diagrams coupled with qRT-PCR showed 305 transcripts differentially expressed by gut ME-M and ME-SW B cells but not splenic ME-SW and MZ B cells compared to naive B cells (Figures 3D–3F and S3A).

This tissue-specific memory signature included increased expression of transcripts for (1) activation-induced receptors such as FcRL4, CD11c (*ITGAX*), and Siglec-6; (2) IgA response-related transcription factors such as RUNX2 and RORA; (3) PC-inducing molecules such as IL-10, IL10RA, CD70, and the transcription factor ZBTB32; and (4) epithelium-targeting chemokine receptors such as CCR1, CCR2, and CCR9 (Figures 3D–3F and S3A; Ehrhardt et al., 2005; Jash

Figure 2. Human Gut ME-M B Cells Inhabit Mucosal Follicles, Show Post-GC Traits, Include a Circulating Counterpart Expressing Gut-Homing Receptors, and Emerge Early in Life

(A) IFA of IgM (green), IgD (red), and DNA (blue) in human ileum tissue sections. Boxes correspond to enlarged right images. Original magnification, 20× (left) or 60× (right). Scale bars, 50 μm.

(B) Number of IgM^+IgD^- ME-M B cells from human intestine calculated by counting cells/mm^2 following tissue IFA. Data summarize results from five different tissue samples where at least four microscopic fields were analyzed.

(C) FCM of CCR7 and CXCR4 on naive, ME-M, and ME-SW B cells from human ileum and colon.

(D) Replication history analyzed by KREC assay. Dashed line corresponds to past cell divisions in control GC B cells from human tonsils.

(E and F) Representative FCM (E) and frequency (F) of human circulating $\beta7^+CCR9^+$ B cells.

(G) IFA of IgM (green), IgD (red), IgA (magenta), and DNA (blue) in intestinal tissues from children. Boxes correspond to enlarged right images. Original magnification, 10× (top left), 20× (top right), 4× (mid left), 40× (mid right), 10× (bottom left), and 40× (bottom right). Scale bars, 50 μm.

Data are from 1 of at least 3 experiments with similar results (A, C, G), summarize 3 experiments (D), or show 1 representative result (E) of 24 experiments (F). Results are presented as mean ± SEM; *$p < 0.05$, **$p < 0.01$, ***$p < 0.001$ (two-tailed unpaired Student's t test). See also Figure S1.

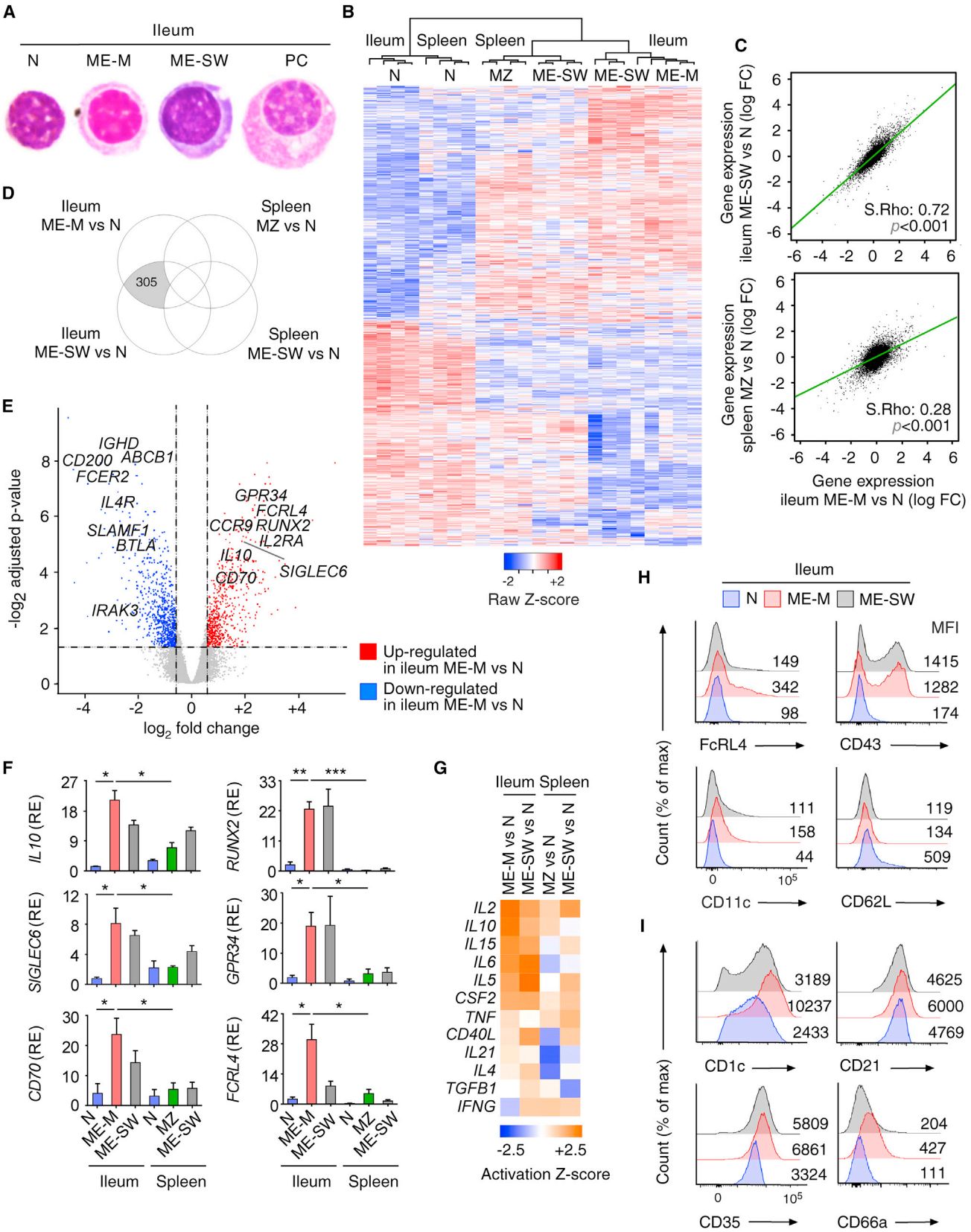

(legend on next page)

et al., 2016; Nair et al., 2016; Rubtsov et al., 2015; Wang et al., 2012; Watanabe et al., 2010). Finally, Ingenuity's upstream regulator analysis indicated that, compared to splenic ME-SW and MZ B cells, gut ME-M and ME-SW B cells expressed functional gene sets predicting enhanced signaling from IL-2, IL-5, IL-6, IL-10, IL-15, and GM-CSF pathways (Figure 3G), which are linked to B cell activation and PC differentiation (Nutt et al., 2015).

Consistent with these data, gut ME-M and ME-SW B cells expressed activation traits encompassing upregulation of FcRL4, CD43, and CD11c combined with downregulation of CD62 ligand expression (Figure 3H). However, compared to gut ME-SW B cells, gut ME-M B cells also showed enhanced MZ-like traits (Figure 3I), including increased expression of CD21, CD35, CD1c, and the adhesion molecule CD66a (Descatoire et al., 2014; Seifert et al., 2015). Notwithstanding these similarities, supervised gene expression analysis, flow cytometry, and gene set enrichment analysis (GSEA) indicated that gut ME-M B cells were distinct from splenic MZ B cells (Figures S3B–S3E). Indeed, gut ME-M B cells expressed less CD84 (Figure S3B), a member of the SLAM family highly expressed by innate-like lymphocytes (Sintes et al., 2010). Furthermore, gut ME-M B cells expressed more gene products implicated in IL-2 and IL-6 receptor signaling via STAT proteins, but fewer gene products implicated in NOTCH signaling (Figures S3C–S3E). Thus, human gut ME-M B cells express a tissue-specific memory gene signature reflecting increased immune activation and PC but not MZ differentiation.

Gut ME-M B Cells Are Clonally Related to PC-Ms and Some PC-As

We next characterized the Ig heavy chain variable (IGHV) and joining (IGHJ) gene repertoires of gut ME-M B cells from paired ileum and colon samples to broadly determine their degree of similarity and diversity with naive B cells and PC-Ms as well as class-switched ME-A B cells and PC-As. Pearson's correlation coefficient analysis of IGHV gene usage indicated that gut ME B cell and PC subsets differed from gut naive B cells but hierarchically clustered with each other based on the expressed isotype, tissue of origin, and cell type (Figures 4A and S4A). The antigen-driven IGHV gene reconfiguration of gut ME B cell and PC subsets was further inferred from their negative selection of IGHV1-18, IGHV1-69, IGHV4-34, and IGHJ6 genes (Figures 4B and S4A) and positive selection of IGHV3-7, IGHV3-23, and IGHJ4 genes (Figures S4A and S4B).

Compared to gut naive B cells, gut ME B cell and PC subsets expressed mutated IGHV genes encoding antigen-binding variable regions with shorter H-CDR3 average length (Figures 4C, S4C, and S4D), two additional hallmarks of antigen-driven selection (Lindner et al., 2012, 2015; Tipton et al., 2015). In addition to these commonalities, gut ME B cell and PC subsets showed significant differences. In particular, ME-M B cells and PC-Ms featured fewer IGHV gene mutations and shorter H-CDR3 compared to ME-A B cells and PC-As from ileum but not colon (Figures 4C, S4C, and S4D). Moreover, ME-M B cells expressed more Ig light chain λ (Igλ) compared to ME-A B cells from ileum but not colon (Figure 4D). These differences could reflect the involvement of ME-M B cells in antigen-driven selection and differentiation programs distinct from those regulating ME-A B cells.

We then investigated the dynamics of the inferred gut antibody repertoire from each donor by collapsing all clones into clonal families and comparing the resulting "core repertoire" to the original "expanded repertoire." Clonal families expressing both IgM and IgA or inhabiting both ileum and colon were expanded compared to the core repertoire, whereas clonal families expressing only IgM or IgA or inhabiting either ileum or colon were not (Figure S4E). These observations indicate that clonal expansion is coupled with increased IgM-to-IgA class switching and intestinal dissemination. We next visualized the ontogenetic affiliations of gut ME-M B cells with other ME B cell and PC subsets through circos plots. While most of these clonally related ME-M B cells were linked to PC-Ms inhabiting identical or distinct gut segments, fewer but large ME-M clonotypes harboring an increased number of IGHV gene mutations were linked to ME-A B cells and/or PC-As (Figures 4E, 4F, S5A, and S5B).

Clonotypic affiliations were further corroborated through the calculation of the Morisita-Horn overlap index, which ascribes 0 and 1 values to unrelated and identical sequences, respectively (Lindner et al., 2015). Ileal ME-M clonotypes showed very robust relatedness with ileal PC-M clonotypes and less robust relatedness with all other subsets clonotypes (Figures 4G and S5C). Further dissection of clonal families through lineage tree reconstruction analysis suggested that some ileal ME-M B cells generate colonic PC-Ms or ileal ME-A B cells upon re-entering GC pathways that induced SHM with or without CSR (Figures 4H and 4I). Additional ileal ME-M B cells from ileum may generate colonic PC-As by entering extra-GC pathways inducing CSR but

Figure 3. Human Gut ME-M B Cells Are Transcriptionally Distinct from Naive B Cells and Express a Tissue-Specific Memory Gene Signature That Includes Multiple Activation Traits

(A) May-Grünwald-Giemsa staining of sorted human intestinal cells. Original magnifications 100×.

(B) Dendrogram of unsupervised agglomerative hierarchical cluster analysis and gene expression heatmap diagram displaying genes differentially expressed by naive, ME-M, and ME-SW B cells sorted from human ileum or naive, MZ, and ME-SW B cells from human spleen.

(C) Scatterplot depicting robust multi-array average normalized expression.

(D) Venn diagram showing transcripts exclusively differentially expressed by ME-M and ME-SW B cells versus naive B cells from human ileum.

(E) Volcano plot representation of genes differentially expressed by ME-M B cells versus naive B cells from human ileum. Selected genes are highlighted.

(F) qRT-PCR of mRNAs encoding selected genes in B cell population as in (B).

(G) Ingenuity's upstream regulator comparison analysis showing selected upstream regulators among cytokine and growth factors differentially expressed (p value > $|\log_{10}5|$).

(H and I) FCM of selected surface molecules on naive, ME-M, and ME-SW B cells from human ileum.

Data are from one of three experiments with similar results (A, H, I), summarize results from four biological replicates (B–E, G), or summarize three independent experiments from at least three different donors (F). Mean ± SEM; *p < 0.05; **p < 0.01; ***p < 0.001 (two-tailed unpaired Student's t test). See also Figures S2 and S3.

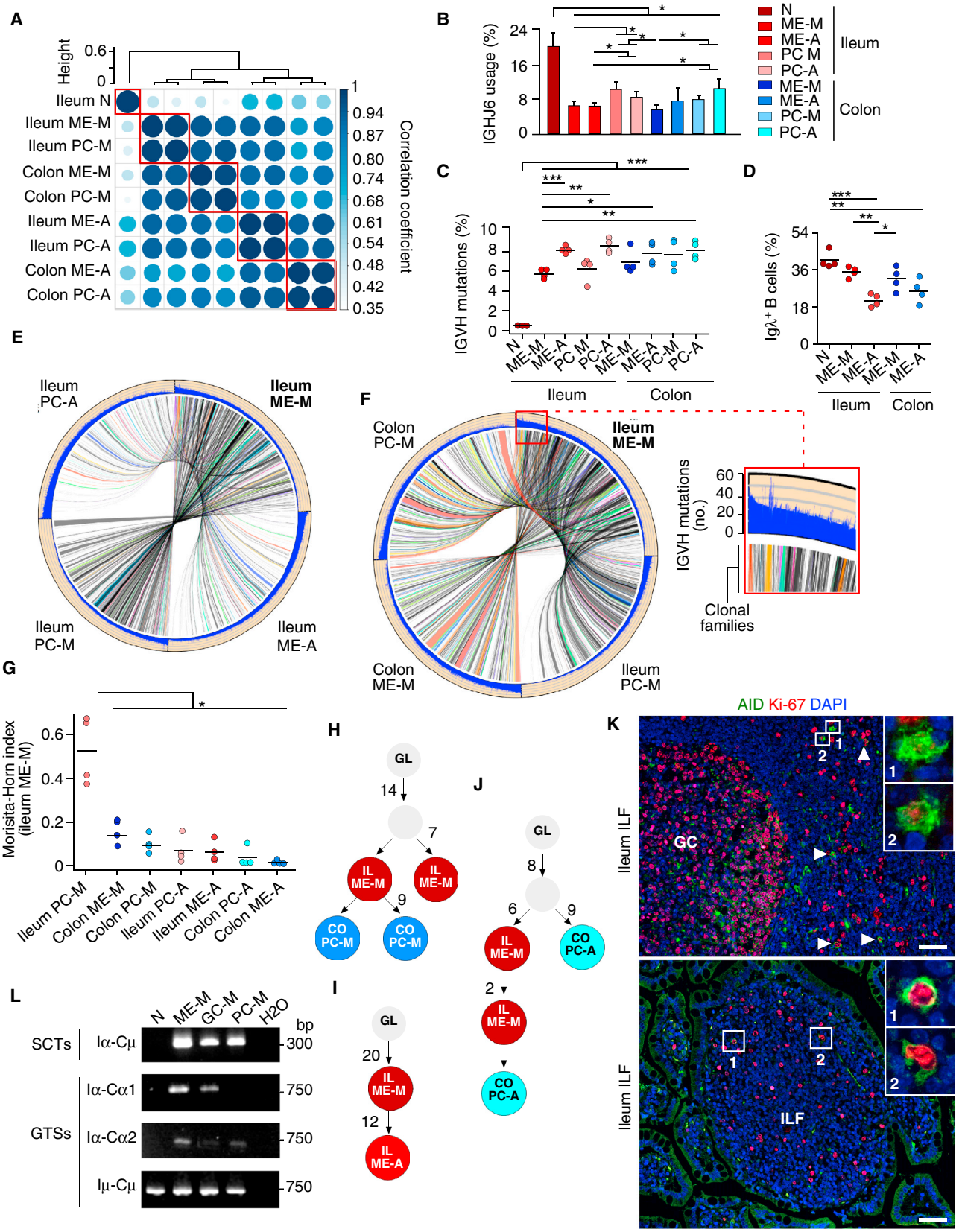

(legend on next page)

not SHM (Figure 4J). Accordingly, tissue immunofluorescence analysis detected B cells expressing the CSR/SHM-inducing enzyme AID and the proliferation molecule Ki-67 in both GC and extra-GC areas from ileum, including ILFs (Figure 4K).

The presence of IgM-to-IgA CSR in some gut ME-M B cells was confirmed by detecting germline Iα1-Cα1 and Iα2-Cα2 as well as switch circle Iα1/2-Cμ transcripts in ME-M but not control naive B cells from human ileum (Figures 4L and S5D). Ileal IgM$^+$ GC B cells predictably contained Iα1-Cα1 and Iα1/2-Cμ, whereas PC-Ms unexpectedly contained Iα1/2-Cμ and Iα2-Cα2 but lacked Iα1-Cα1 (Figure 4L). These PC-Ms may emerge from recently activated ME-M clones concomitantly receiving IgM-to-IgA CSR-inducing signals. Thus, human ME-M B cells disseminate to both ileum and colon and may differentiate to PC-Ms and class-switched PC-As by re-entering GCs or progressing through extra-GC pathways.

Gut ME-M B Cells Secrete IgM and Switch to IgA upon TD or TI Stimulation

The differentiation potential of human gut ME-M B cells was further explored by evaluating their proliferation, CSR and PC differentiation upon exposure to TD (CD40L and IL-21) or TI (CpG DNA combined or not with BAFF and APRIL) signals. IL-10 was supplemented to maximize CSR and PC differentiation (Macpherson et al., 2008).

As shown by CFSE dilution assays, TD signals induced comparable proliferation of gut ME-M and naive B cells, whereas TI signals induced proliferation of gut ME-M but not naive B cells, particularly in the presence of BAFF and APRIL (Figures 5A and 5B). Moreover, ME-M B cells differentiated into proliferating CD38^{hi}CFSE^{lo} plasmablasts in response to either TD or TI signals, whereas naive B cells did so only in response to TD signals (Figure 5C). Of note, a sizable fraction of plasmablasts emerging from activated ME-M but not naive B cells expressed IgA but lacked IgM (Figure 5D).

Consistent with these data, ME-M B cells secreted copious IgM and less abundant IgA in response to TD or TI signals, whereas naive B cells showed weaker IgM and IgA responses to TD but not TI signals (Figure 5E). We then wondered whether CSR targeted gut ME-M B cells expressing FcRL4, which defines activated tissue-based memory B cells (Ehrhardt et al., 2005). Indeed, TD signals generated plasmablasts from both FcRL4$^-$ and FcRL4$^+$ ME-M B cells, but induced IgM-to-IgA CSR only in FcRL4$^+$ ME-M B cells (Figure 5F). Accordingly, gut FcRL4$^+$ but not FcRL4$^-$ ME-M B cells contained transcripts for the CSR (and SHM)-inducing enzyme AID (Figure 5G). Thus, human gut ME-M B cells proliferate and generate PC-Ms in response to TD or TI signals, which further induce IgM-to-IgA CSR in the FcRL4$^+$ fraction of ME-M B cells.

Gut ME-M B Cells and PC-Ms Release IgM to Mucus-Embedded Commensals

We next developed an EBV-based protocol to determine whether human gut ME-M B cells produced IgM to autologous mucus-embedded bacteria (Figure 6A). Initial ELISAs showed that IgM from ileal ME-M B cells recognized commensal antigens such as phosphorylcholine, β-glucan, laminarin, galactose-α-1,3-galactose, and capsular polysaccharides, whereas IgM from ileal naive B cells did not (Figures 6B and S6A). Further flow cytometry assays showed that IgM from ileal ME-M B cells recognized mucus-embedded commensals more efficiently than IgM from ileal naive B cells did (Figure 6C).

We then quantified binding of PC-derived SIgM to mucus-embedded microbiota from paired human ileum and colon samples (Figures 6D, S6B, and S6C). Initial ELISAs detected free SIgM in mucus, though in lesser amounts than free SIgA (Figure 6E). Most mucus samples included significant SIgA$^+$SIgM$^+$, SIgA$^+$SIgM$^-$, and SIgA$^-$SIgM$^-$ but negligible SIgA$^-$SIgM$^+$ microbiota fractions (Figure 6F). The frequency of these fractions was variable among individuals and between ileum and colon from the same individual. Consistent with the virtual lack of PC-Ms in the murine gut and published results (Bunker et al., 2015), the microbiota from the small and large intestines of wild-type mice included IgA$^-$SIgM$^-$ and SIgA$^+$SIgM$^-$ but not SIgA$^+$SIgM$^+$ bacterial fractions (Figure 6G). Enhancing gut microbiota complexity by housing mice outside the specific pathogen-free (SPF) barrier increased neither SIgA$^+$SIgM$^+$ bacteria nor PC-Ms nor PC-As, but did increase SIgA$^+$SIgM$^-$ bacteria (Figures S6D and S6E). Thus, human gut ME-M B cells recognize commensals as clonally related PC-Ms do. These latter generate homeostatic SIgM responses that target SIgA-coated bacteria in humans but not wild-type mice.

SIgM from Gut PC-Ms Binds Highly Diverse Commensals Dually Coated by SIgA

We next devised a strategy to profile mucus-embedded bacteria from human ileum or colon by 16S ribosomal RNA (rRNA) gene sequencing and found inter-individual variability

Figure 4. Human Gut ME-M B Cells Express a Post-GC Mutational Profile and Clonally Relate to Gut PC-Ms and Some PC-As

(A) Pearson's correlation coefficient matrix of IGHV gene usage by naive B cells and paired ME-M B cells, ME-A B cells, PC-Ms, and PC-As from human ileum or colon grouped by hierarchical clustering algorithm according to common gene set usage. Circle size and color saturation indicate correlation strength.

(B and C) Relative mean frequency of IGHJ6 gene usage and mean number of IGHV gene mutations per 100 bp in gut B cell and PC subsets as in (A).

(D) Frequency of Igλ-expressing cells calculated by FCM.

(E and F) Circos plots depicting clonal relationships and IGHV gene mutations.

(G) Morisita-Horn index showing clonal repertoire overlap between ME-M B cells from human ileum and all other B cell subsets as in (A).

(H–J) Lineage tree reconstruction of inferred clonal families (colored circles) and their inferred germline (GL) and intermediate precursors (gray circles). Edges and numbers indicate mutations accumulated along the lineage tree.

(K) IFA of ILFs from human ileum stained for AID (green), Ki-67 (red), and DNA (blue). Insets correspond to boxed areas in main images. Original magnification, 20× (top) or 40× (bottom). Scale bars, 50 μm.

(L) PCR of switch circle Iα-Cμ transcripts (SCTs) as well as germline Iμ-Cμ, Iα-Cα1, and Iα-Cα2 transcripts (GTs) in naive, ME-M, and IgM$^+$ GC B cells or PC-Ms from human ileum.

Data are from 1 representative donor (E, F, H–L) or summarize results from 4 different donors (A–D, G). Error bars, SD; *$p < 0.05$, **$p < 0.01$, ***$p < 0.001$ (Welch's t test and one-way ANOVA with Tukey's post hoc test). See also Figures S4 and S5.

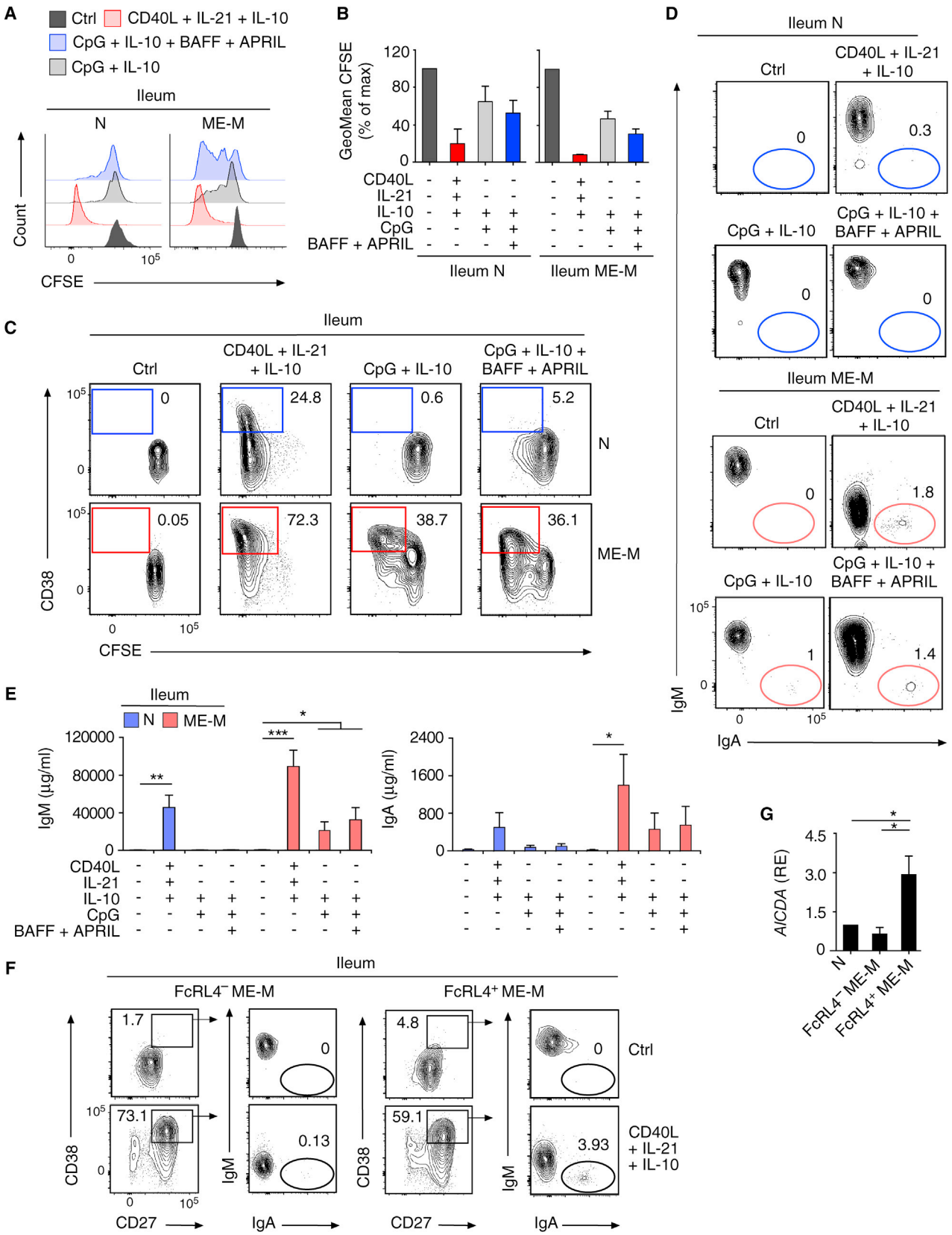

(legend on next page)

at phylum and genus levels (Figures S7A–S7C). Differences in bacterial composition between ileum and colon from the same donor were less pronounced than between donors, as shown by unsupervised hierarchical clustering (Figure S7C). Rarefaction plots calculating Faith's phylogenetic diversity and Shannon index confirmed that phylogenetic richness and species diversity varied among donors but not between tissues (Figures S7D and S7E).

To comparatively profile SIgA$^+$SIgM$^+$, SIgA$^+$SIgM$^-$, and SIgA$^-$SIgM$^-$ fractions of mucus-embedded bacteria in a comprehensive and unbiased manner, we combined SIgM/A-based sorting with 16S rRNA gene sequencing (Figure 7A). The composition of each fraction varied at both phylum and genus levels, though all fractions showed more Bacteroidetes and Firmicutes than Proteobacteria and Actinobacteria (Figures 7B and 7C). Also, phylogenetic richness and microbial species diversity varied among fractions, with an overall decrease from SIgA$^+$SIgM$^+$ to SIgA$^+$SIgM$^-$ and SIgA$^-$SIgM$^-$ fractions (Figure 7D). This finding correlated with differences in phylum composition, including proportionally fewer Bacteroidetes but more Firmicutes in SIgA$^+$SIgM$^+$ compared to SIgA$^+$SIgM$^-$ and SIgA$^-$SIgM$^-$ fractions (Figure 7E).

To identify microbial species accounting for the above phylum differences at the operational taxonomic unit (OTU) level, we used a log-based enrichment index (Figure 7F). A hierarchical clustering algorithm applied to a conservative selection of OTU-based enrichment indexes showed that SIgA$^+$SIgM$^+$ and SIgA$^+$SIgM$^-$ fractions grouped together, separately from the SIgA$^-$SIgM$^-$ fraction (Figure 7F). Of twelve OTUs showing a significantly different enrichment index, seven *Lachnospiraceae* and *Ruminococcaceae* were enriched in SIgA$^+$SIgM$^+$ compared to SIgA$^-$SIgM$^-$ bacteria (Figures 7F and S7F).

Accordingly, flow cytometry-based coating assays determined that IgM from EBV-transformed gut ME-M B cell lines strongly bound Firmicutes such as *Bacillus cereus*, *Roseburia intestinalis* (belonging to *Lachnospiraceae*), and *Ruthenibacterium lactatiformans* (belonging to *Ruminococcaceae*). In addition, IgM showed elevated binding to Bacteroidetes such as *Bacteroides vulgatus*, but little or no binding to other Bacteroidetes or Proteobacteria such as *Bacteroides fragilis*, *Bacteroides thetaiotamicron*, and *Escherichia coli* (Figure S7G). Thus, human SIgM may cooperate with SIgA to implement mucus retention of diverse microbial communities, including Firmicutes with putative beneficial functions.

DISCUSSION

We have shown that human gut PC-Ms were clonally related to a large and previously unrecognized repertoire of ME-M B cells that predominantly inhabited gut-associated follicles. Besides undergoing IgM-to-IgA CSR in response to TD or TI signals, gut ME-M B cells secreted abundant IgM, which, along with SIgM, recognized mucus-embedded commensals. Of note, SIgM-coated bacteria were dually targeted by SIgA and showed increased diversity and distinct composition compared to uncoated or SIgA-only-coated bacteria. Thus, SIgM may help SIgA to anchor non-redundant microbial communities to mucus.

The key role of SIgA in gut homeostasis can be inferred from the emergence of dysbiosis in mice lacking B cells, IgA, AID, or pIgR (Kubinak and Round, 2016). In addition to dysbiosis, patients with antibody deficiency can develop gut inflammation, including inflammatory bowel disease (Agarwal and Mayer, 2009). This complication is more frequent in common variable immunodeficiency cases with combined SIgM and SIgA depletion (Agarwal and Mayer, 2009), suggesting that human gut homeostasis requires microbiota targeting by both SIgM and SIgA. Accordingly, we found that PC-Ms accumulated in the human but not mouse gut mucosa and further demonstrated that SIgM coated human but not mouse gut bacteria in combination with SIgA.

Remarkably, human gut PC-Ms established extensive clonal relationships with a large repertoire of gut ME-M B cells that were rare in systemic or mucosal extra-intestinal lymphoid organs, including spleen and tonsils. The prominent gut tropism of ME-M B cells was further indicated by studies showing robust $\alpha4\beta7$ and CCR9 co-expression on a large fraction of circulating ME-M B cells and PC-Ms. Of note, $\alpha4\beta7$ and CCR9 induction mostly occurs in lymphoid structures from the small intestine and promotes migration of gut ME-A B cells and immature PC-As to the small intestinal LP (Macpherson et al., 2008). Accordingly, gut ME-M B cells predominantly inhabited Peyer's patches and ILFs from the small intestinal mucosa, whereas PC-Ms mostly accumulated in the small intestinal LP. Similar to PC-As, gut ME-M B cells and PC-Ms became detectable as early as 1.5 months after birth. While PC-Ms further accumulated over the first 10 years of life, ME-M B cells remained numerically stable over time. These results suggest that SIgM may shape the microbiota of a developing individual in cooperation with SIgA (Planer et al., 2016).

Our identification of clonally related ME-M B cells and PC-Ms in the human gut extends evidence from mouse systemic

Figure 5. Human Gut ME-M B Cells Undergo Proliferation, PC Differentiation, IgM Secretion, and IgA Class Switching in Response to TD or TI Signals

(A and B) FCM of CFSE dilution profiles (A) and GeoMean (% of max) of CFSE staining (B) in naive (N) and ME-M B cells from human ileum cultured for 5 days as indicated. Ctrl, medium alone.

(C) FCM of CFSE and CD38 on naive (top) and ME-M (bottom) B cells from human ileum cultured as in (A) and (B). Numbers indicate percent of newly formed CD38^{hi}CFSE^{lo} PCs.

(D) FCM of IgM and IgA on CD38^{hi}CFSE^{lo} plasmablasts emerging upon stimulation as in (A) and (B).

(E) ELISA of IgM and IgA secreted by naive (N) and ME-M B cells from human ileum cultured for 5–7 days as in (A) and (B).

(F) FCM of CD38, CD27, IgM, and IgA on sorted FcRL4$^-$ (left) or FcRL4$^+$ (right) ME-M B cells from human ileum cultured for 5 days with medium alone (ctrl) or CD40L, IL-21, and IL-10.

(G) qRT-PCR analysis of mRNA encoding AID (*AICDA*) in naive, FcRL4$^-$ ME-M, and FcRL4$^+$ ME-M B cells from human ileum.

Data represent one representative experiment of two with similar results (A–D, F) or summarize at least three different experiments (E, G). Results are presented as mean ± SEM; *$p < 0.05$, **$p < 0.01$, ***$p < 0.001$ (two-tailed unpaired Student's t test).

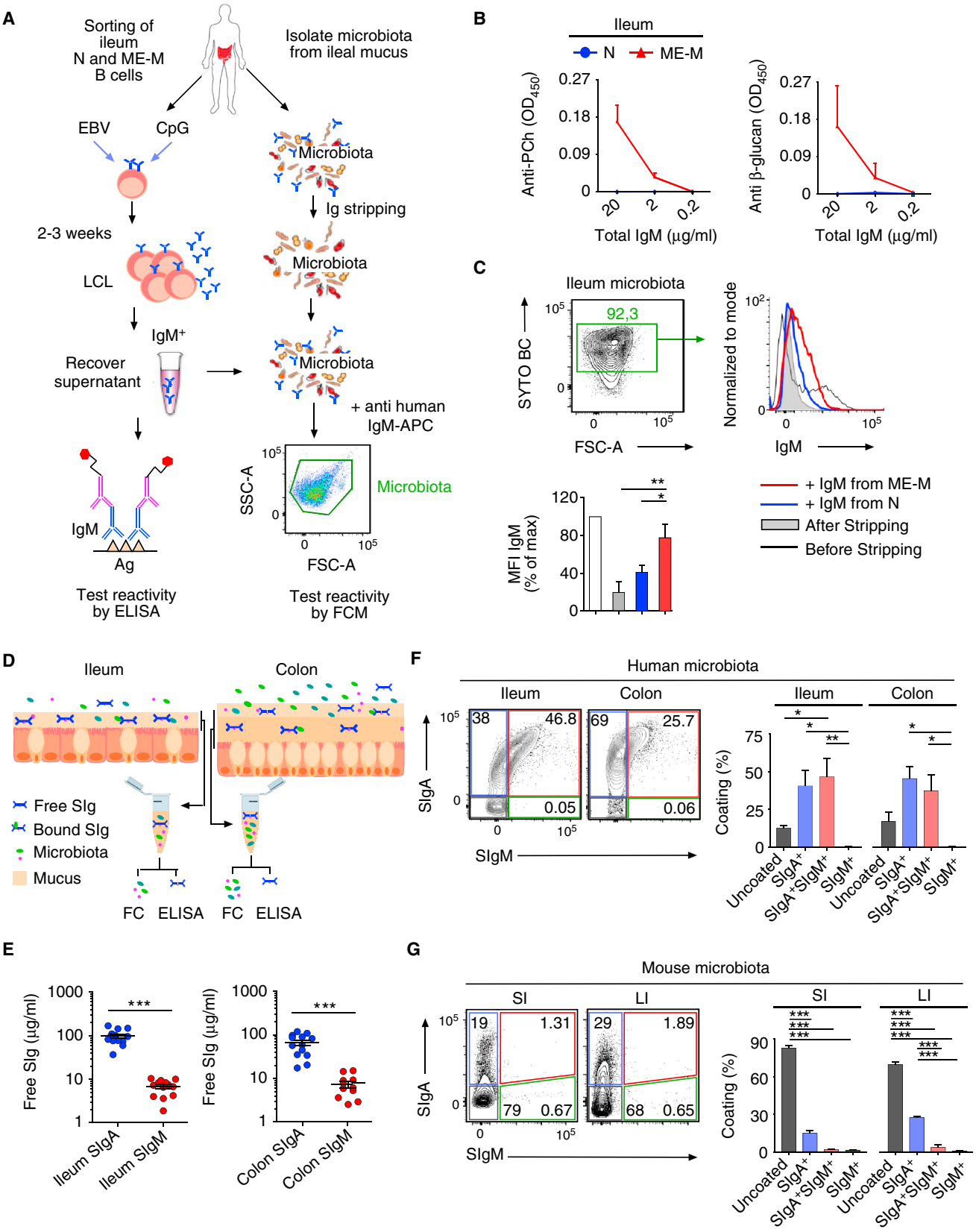

(legend on next page)

immunization models indicating that humoral memory is not merely comprised of ME-G and ME-A B cells, but further extends to ME-M B cells (Dogan et al., 2009; Kurosaki et al., 2015; Pape et al., 2011). Besides expressing canonical memory molecules such as CD24, CD27, and CD148, human gut ME-M B cells featured post-GC expression of mutated IGHV genes and negative selection of IGHV1-69, IGHV4-34, and IGHJ6 genes, which encode antibodies enriched in self-reactivity (Tipton et al., 2015). Furthermore, some ME-M B cells showed clonal properties consistent with re-entry into GC pathways promoting SHM in addition to PC-M differentiation.

Diversification of human gut PC-Ms from pre-existing memory specificities echoes works showing homeostatic or immunization-induced diversification of gut ME-A B cells in GCs from Peyer's patches (Bemark et al., 2016; Lindner et al., 2012, 2015). In addition to PC-Ms, human gut ME-M B cells generated some ME-A B cells and PC-As by entering either GC pathways coupled with SHM and CSR or GC-independent pathways promoting CSR but not SHM. This conclusion was supported by lineage tree reconstruction analysis of high-throughput IGHV gene sequencing data, detection of AID in activated FcRL4$^+$ gut ME-M B cells responsive to IgM-to-IgA CSR-inducing signals, identification of IgM-to-IgA CSR in unfractioned ME-M B cells, and detection of AID in B cells from both GC and extra-GC areas.

In mice, systemic ME-G and ME-M B cells were thought to rapidly induce PC-Gs or a secondary GC reaction upon re-exposure to antigen, respectively (Dogan et al., 2009; Pape et al., 2011). This view has been modified by mouse studies indicating that systemic ME-M B cells can rapidly differentiate into IgG class-switched plasmablasts in response to TI or TD signals (Krishnamurty et al., 2016; Zuccarino-Catania et al., 2014). Accordingly, human intestinal ME-M B cells progressed along intertwined GC-dependent and GC-independent pathways that promoted IgM-to-IgA CSR in addition to PC differentiation. Compared to gut naive B cells, which showed weaker and TD-biased antibody responses, gut ME-M B cells comparably induced plasmablasts secreting IgM or IgA in response to either TD or TI signals. Of note, similar signals activate rotavirus-specific gut ME-M B cells (Narváez et al., 2012). Local TD and TI cues could further imprint ME-M B cells with a tissue-specific memory signature similar to that described in tonsillar ME-G/A B cells (Ehrhardt et al., 2005). This signature included CD11c, Siglec-6, CCR9, IL-10, IL-10Rα, and RORα upregulation, which reflects non-inflammatory activation and mucosal homing.

Gut ME-M B cells also expressed a common memory signature shared with gut and splenic ME-SW B cells. This signature included FcRL4 and TACI upregulation, which suggests increased activation by TI signals from TLR ligands and BAFF or APRIL (He et al., 2010; Sohn et al., 2011), as well as CD72, FOXO1, BACH2, and BTLA4 downregulation, which reflects increased propensity to undergo proliferation and PC differentiation (Kurosaki et al., 2015). Similar to splenic MZ B cells, gut ME-M B cells expressed more CD1c, CD21, CD35, and CD66a compared to gut ME-SW B cells, a finding reminiscent of recent studies suggesting that splenic MZ B cells originate from gut precursors (Vossenkämper et al., 2013). However, the global transcriptome of gut ME-M B cells clustered separately from that of splenic MZ B cells. Compared to these latter, gut ME-M B cell expressed less CD84, more gene products linked to PC-inducing IL-2 and IL-6 signaling, and fewer gene products linked to NOTCH signaling, which is required for MZ B cell differentiation (Descatoire et al., 2014).

Besides establishing affiliations with IgM$^+$ and IgA$^+$ clonotypes, ME-M B cells formed a core repertoire of clonally organized families that emerged early in life and did not show age-dependent accumulation. Thus, ME-M B cells may form a stable but functionally plastic pool of "immune sentinels" within sites of antigen entry, such as ILFs. These sites contained two parallel repertoires of unswitched ME-M and naive B cells expressing follicle-targeting CCR7 and CXCR4 receptors. As indicated by their unique phenotypic, molecular, transcriptional, and functional traits, these B cell subsets may offer unique solutions to different problems. While ME-M B cells may initiate quickly developing SIgM and SIgA responses to rapidly match transient changes of the microbiota, naive B cells may induce de novo SIgM and SIgA responses to counter more durable microbial perturbations. Consistent with their involvement in the homeostatic control of commensals, ME-M B cells produced IgM to mucus-embedded bacteria as SIgM from clonally related PC-Ms did.

The presence of homeostatic SIgM responses in humans but not mice may reflect the lower complexity of the mouse gut microbiota (Kamada et al., 2013). However, neither PC-Ms nor SIgM-coated bacteria increased in non-SPF mice harboring a more complex microbiota, suggesting that B cell-intrinsic differences also play a role. Accordingly, ME-M B cells from orally immunized mice have been shown to colonize the spleen and bone marrow but not gut follicles (Bemark et al., 2016). Remarkably, SIgM coated a fraction of the human microbiota that was also targeted by SIgA. Compared to uncoated or SIgA-only-coated bacteria, bacteria dually coated by SIgM and SIgA showed increased diversity, a parameter linked to gut homeostasis (Kamada et al., 2013). By activating complement (Kirkland

Figure 6. Human IgM from Gut ME-M B Cells and SIgM from Gut PC-Ms Target Mucus-Embedded Commensals, Including Bacteria Dually Coated by SIgA

(A) Strategy used to test reactivity of IgM secreted by human ME-M B cells and control naive (N) B cells from human ileum. LCL, lymphoblastoid cell line.
(B) ELISA measuring reactivity for phosphorylcholine (PCh) and β-glucan of IgM secreted by EBV-transformed naive or ME-M B cells from human ileum.
(C) Reactivity of IgM from naive (N) or ME-M B cells to SYTO BC$^+$ mucus-embedded microbiota.
(D) Experimental strategy used to measure free and microbiota-bound SIgM and SIgA from human gut mucus.
(E) ELISA of free SIgM (blue) and SIgA (red) in mucus samples.
(F and G) FCM of SIgA and SIgM bound to viable SYTO BC$^+$ microbiota from human ileum or colon mucus (F) or from small intestine (SI) and large intestine (LI) lumen of wild-type C57BL/6 mice housed under SPF conditions (G).
Data summarize at least 3 (B, C, bottom graph), 12 (E), or 20 (F, G, right graphs) experiments in addition to showing results from one representative experiment (C, cytogram and profiles; F, G left cytograms). Two-tailed paired Student's t test (C, E) and one-way ANOVA with Tukey's post hoc test (F, G). Results are presented as mean ± SEM; *$p < 0.05$, **$p < 0.01$, ***$p < 0.001$. See also Figure S6.

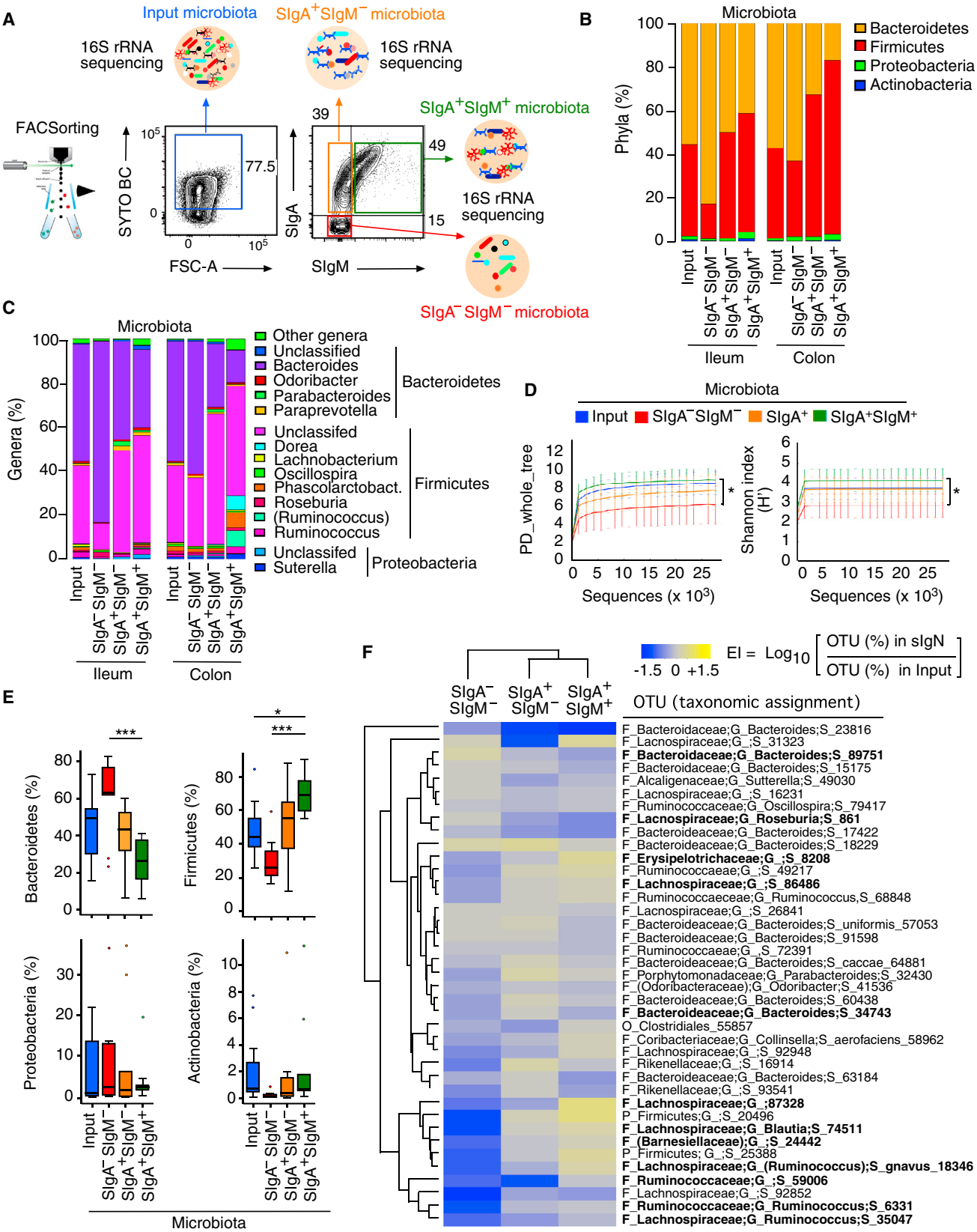

(legend on next page)

et al., 2012), SIgM may constrain the growth of common commensals, thereby helping SIgA to optimize microbiota diversity (Kubinak and Round, 2016). Accordingly, SIgA deficiency causes dysbiosis and inflammatory bowel disease when combined with SIgM deficiency, as in patients with common variable immunodeficiency (Agarwal and Mayer, 2009).

Compared to uncoated bacteria, bacteria dually coated by SIgM and SIgA as well as bacteria coated by SIgA alone were enriched in Firmicutes, including *Lachnospiraceae* and *Ruminococcaceae*. By degrading dietary polysaccharides into short-chain fatty acids with immunoregulatory and SIgA-inducing functions (Arpaia et al., 2013; Kim et al., 2016), these commensals may enhance protection against obesity and infection (Biddle et al., 2013; Cho et al., 2012; Petrof et al., 2013). Should this be the case, PC-Ms and clonally related PC-As may maximize gut retention of non-redundant microbial consortia through a mechanism involving mucus interaction with the pIgR-derived secretory fragment of SIgM and SIgA (Macpherson et al., 2008). This dual anchoring strategy may have evolved to preserve microbiota homeostasis under common pathological conditions selectively depleting SIgA. Similar to a large fraction of gut IgA (Benckert et al., 2011), gut IgM showed evidence of polyreactivity, because it targeted common microbial products and some Bacteroidetes such as *Bacteroides vulgatus* in addition to Firmicutes. In summary, SIgM may emerge from pre-existing memory rather than newly activated naive IgM^+ B cells and could help SIgA to select, control, and retain highly diverse and putatively beneficial commensal communities within gut mucus.

STAR★METHODS

Detailed methods are provided in the online version of this paper and include the following:

- KEY RESOURCES TABLE
- CONTACT FOR REAGENT AND RESOURCE SHARING
- EXPERIMENTAL MODEL AND SUBJECT DETAILS
  - Human Tissue and Blood Specimens
  - Mice
- METHOD DETAILS
  - Sample Processing
  - Flow Cytometry
  - Cell Sorting
  - Cell Cultures
  - Proliferation Assay
  - Generation of EBV-Transformed B Cells
  - ELISA
  - Immunofluorescence Analysis
  - Giemsa Staining
  - RNA Extraction and Reverse Transcription
  - Quantitative Real Time and Standard PCR
  - KREC Assay
  - Global Transcriptome Analysis
  - Next Generation Sequencing of Ig Gene Repertoires
  - Mucus Collection and Processing
  - Bacterial Flow Cytometry and FACSorting
  - Bacterial 16S rRNA Gene Analysis
  - Quantification and Statistical Analysis
- DATA AND SOFTWARE AVAILABILITY

SUPPLEMENTAL INFORMATION

Supplemental Information includes seven figures and four tables and can be found with this article online at http://dx.doi.org/10.1016/j.immuni.2017.06.013.

AUTHOR CONTRIBUTIONS

G.M. and L.C. designed and performed experiments, analyzed results, discussed data, and wrote the manuscript; M.P. designed experiments, analyzed and discussed sequencing data, and wrote the manuscript; J.S. performed research, analyzed results, and discussed data; D.L., D.S.-G., S.B., A.Y., and M.U. performed experiments; C.G., E.K.G., and M.R. discussed the data; M.C.V.Z. and E.M. provided essential reagents and discussed data; R.A.-G., I.V., M.I., S.S., and L.M. provided tissue and microbiota samples; S.M. designed experiments and discussed data; and A.C. designed experiments, discussed data, and wrote the manuscript.

ACKNOWLEDGMENTS

We thank the Microarray Analysis Service from IMIM for global gene transcriptome analysis, the Genomic Core Facility from UPF and Christopher M. Tipton from Emory University for help with NGS, and the FACS Unit from UPF and CRG for help with cell sorting. Supported by European Advanced Grant (ERC-2011-ADG-20110310), MINECO (SAF2014-52483-R), AGAUR (2014 SGR 832), US NIH grants P01 AI61093, R01 AI57653, and U01 AI95613 (to A.C.), Boeringher Ingelheim grant 134564-2 (to A.C.), NIH grant R01 DK 112296-01 (to A.C. and S.M.), and Fondo de Investigación Sanitaria ISCIII fellowships CD14/00060 and CM13/00136 (to G.M. and L.C., respectively).

Received: December 22, 2016
Revised: April 7, 2017
Accepted: June 16, 2017
Published: July 11, 2017

REFERENCES

Agarwal, S., and Mayer, L. (2009). Pathogenesis and treatment of gastrointestinal disease in antibody deficiency syndromes. J. Allergy Clin. Immunol. *124*, 658–664.

Figure 7. Human Mucus-Embedded Commensals Dually Coated by SIgM and SIgA Show Increased Richness and Diversity Compared to Uncoated or SIgA-Only-Coated Commensals

(A) Strategy used to profile mucus-embedded microbiota from human ileum or colon by 16S rRNA gene sequencing following IgM/A sorting.
(B and C) Relative abundance of phyla (B) and genera (C) in microbiota fractioned as in (A). Top 15 most abundant genera are depicted.
(D) Rarefaction plots depicting phylogenetic richness (left; calculated by PD_whole_tree) and species diversity (right; calculated by Shannon index) of microbiota fractioned as in (A). Mean ± SD.
(E) Boxplot distribution of mean relative abundance of phyla from bacteria fractioned as in (A).
(F) Heatmap diagram of mean enrichement index (EI) among donors at the OTU level. Hierarchical clustering was used to group fractions and OTUs. OTUs with significantly different EI among fractions are shown in bold.
Data are from one sequencing dataset from two different gut segments of one representative donor (B and C) or summarize 10 sequencing datasets from two different gut segments of 5 donors (D–F). *$p < 0.05$, **$p < 0.01$, ***$p < 0.001$ (Welch's t test). See also Figure S7.

Aranburu, A., Piano Mortari, E., Baban, A., Giorda, E., Cascioli, S., Marcellini, V., Scarsella, M., Ceccarelli, S., Corbelli, S., Cantarutti, N., et al. (2017). Human B-cell memory is shaped by age- and tissue-specific T-independent and GC-dependent events. Eur. J. Immunol. *47*, 327–344.

Arpaia, N., Campbell, C., Fan, X., Dikiy, S., van der Veeken, J., deRoos, P., Liu, H., Cross, J.R., Pfeffer, K., Coffer, P.J., and Rudensky, A.Y. (2013). Metabolites produced by commensal bacteria promote peripheral regulatory T-cell generation. Nature *504*, 451–455.

Barak, M., Zuckerman, N.S., Edelman, H., Unger, R., and Mehr, R. (2008). IgTree: creating Immunoglobulin variable region gene lineage trees. J. Immunol. Methods *338*, 67–74.

Bemark, M., Hazanov, H., Strömberg, A., Komban, R., Holmqvist, J., Köster, S., Mattsson, J., Sikora, P., Mehr, R., and Lycke, N.Y. (2016). Limited clonal relatedness between gut IgA plasma cells and memory B cells after oral immunization. Nat. Commun. *7*, 12698.

Benckert, J., Schmolka, N., Kreschel, C., Zoller, M.J., Sturm, A., Wiedenmann, B., and Wardemann, H. (2011). The majority of intestinal IgA+ and IgG+ plasmablasts in the human gut are antigen-specific. J. Clin. Invest. *121*, 1946–1955.

Berkowska, M.A., Driessen, G.J., Bikos, V., Grosserichter-Wagener, C., Stamatopoulos, K., Cerutti, A., He, B., Biermann, K., Lange, J.F., van der Burg, M., et al. (2011). Human memory B cells originate from three distinct germinal center-dependent and -independent maturation pathways. Blood *118*, 2150–2158.

Biddle, A., Stewart, L., Blanchard, J., and Leschine, S. (2013). Untangling the genetic basis of fibrolytic specialization by Lachnospiraceae and Ruminococcaceae in diverse gut communities. Diversity (Basel) *5*, 627–640.

Bunker, J.J., Flynn, T.M., Koval, J.C., Shaw, D.G., Meisel, M., McDonald, B.D., Ishizuka, I.E., Dent, A.L., Wilson, P.C., Jabri, B., et al. (2015). Innate and adaptive humoral responses coat distinct commensal bacteria with immunoglobulin A. Immunity *43*, 541–553.

Caporaso, J.G., Kuczynski, J., Stombaugh, J., Bittinger, K., Bushman, F.D., Costello, E.K., Fierer, N., Peña, A.G., Goodrich, J.K., Gordon, J.I., et al. (2010). QIIME allows analysis of high-throughput community sequencing data. Nat. Methods *7*, 335–336.

Cho, I., Yamanishi, S., Cox, L., Methé, B.A., Zavadil, J., Li, K., Gao, Z., Mahana, D., Raju, K., Teitler, I., et al. (2012). Antibiotics in early life alter the murine colonic microbiome and adiposity. Nature *488*, 621–626.

Descatoire, M., Weller, S., Irtan, S., Sarnacki, S., Feuillard, J., Storck, S., Guiochon-Mantel, A., Bouligand, J., Morali, A., Cohen, J., et al. (2014). Identification of a human splenic marginal zone B cell precursor with NOTCH2-dependent differentiation properties. J. Exp. Med. *211*, 987–1000.

Dogan, I., Bertocci, B., Vilmont, V., Delbos, F., Mégret, J., Storck, S., Reynaud, C.A., and Weill, J.C. (2009). Multiple layers of B cell memory with different effector functions. Nat. Immunol. *10*, 1292–1299.

Ehrhardt, G.R., Hsu, J.T., Gartland, L., Leu, C.M., Zhang, S., Davis, R.S., and Cooper, M.D. (2005). Expression of the immunoregulatory molecule FcRH4 defines a distinctive tissue-based population of memory B cells. J. Exp. Med. *202*, 783–791.

Gupta, N.T., Vander Heiden, J.A., Uduman, M., Gadala-Maria, D., Yaari, G., and Kleinstein, S.H. (2015). Change-O: a toolkit for analyzing large-scale B cell immunoglobulin repertoire sequencing data. Bioinformatics *31*, 3356–3358.

He, B., Santamaria, R., Xu, W., Cols, M., Chen, K., Puga, I., Shan, M., Xiong, H., Bussel, J.B., Chiu, A., et al. (2010). The transmembrane activator TACI triggers immunoglobulin class switching by activating B cells through the adaptor MyD88. Nat. Immunol. *11*, 836–845.

Jash, A., Wang, Y., Weisel, F.J., Scharer, C.D., Boss, J.M., Shlomchik, M.J., and Bhattacharya, D. (2016). ZBTB32 restricts the duration of memory B cell recall responses. J. Immunol. *197*, 1159–1168.

Kamada, N., Seo, S.U., Chen, G.Y., and Núñez, G. (2013). Role of the gut microbiota in immunity and inflammatory disease. Nat. Rev. Immunol. *13*, 321–335.

Kawamoto, S., Maruya, M., Kato, L.M., Suda, W., Atarashi, K., Doi, Y., Tsutsui, Y., Qin, H., Honda, K., Okada, T., et al. (2014). Foxp3(+) T cells regulate immunoglobulin a selection and facilitate diversification of bacterial species responsible for immune homeostasis. Immunity *41*, 152–165.

Kim, M., Qie, Y., Park, J., and Kim, C.H. (2016). Gut microbial metabolites fuel host antibody responses. Cell Host Microbe *20*, 202–214.

Kirkland, D., Benson, A., Mirpuri, J., Pifer, R., Hou, B., DeFranco, A.L., and Yarovinsky, F. (2012). B cell-intrinsic MyD88 signaling prevents the lethal dissemination of commensal bacteria during colonic damage. Immunity *36*, 228–238.

Klein, U., Rajewsky, K., and Küppers, R. (1998). Human immunoglobulin (Ig)M+IgD+ peripheral blood B cells expressing the CD27 cell surface antigen carry somatically mutated variable region genes: CD27 as a general marker for somatically mutated (memory) B cells. J. Exp. Med. *188*, 1679–1689.

Krishnamurty, A.T., Thouvenel, C.D., Portugal, S., Keitany, G.J., Kim, K.S., Holder, A., Crompton, P.D., Rawlings, D.J., and Pepper, M. (2016). Somatically hypermutated *Plasmodium*-specific IgM(+) memory B cells are rapid, plastic, early responders upon malaria rechallenge. Immunity *45*, 402–414.

Kubinak, J.L., and Round, J.L. (2016). Do antibodies select a healthy microbiota? Nat. Rev. Immunol. *16*, 767–774.

Kurosaki, T., Kometani, K., and Ise, W. (2015). Memory B cells. Nat. Rev. Immunol. *15*, 149–159.

Lindner, C., Wahl, B., Föhse, L., Suerbaum, S., Macpherson, A.J., Prinz, I., and Pabst, O. (2012). Age, microbiota, and T cells shape diverse individual IgA repertoires in the intestine. J. Exp. Med. *209*, 365–377.

Lindner, C., Thomsen, I., Wahl, B., Ugur, M., Sethi, M.K., Friedrichsen, M., Smoczek, A., Ott, S., Baumann, U., Suerbaum, S., et al. (2015). Diversification of memory B cells drives the continuous adaptation of secretory antibodies to gut microbiota. Nat. Immunol. *16*, 880–888.

Macpherson, A.J., McCoy, K.D., Johansen, F.E., and Brandtzaeg, P. (2008). The immune geography of IgA induction and function. Mucosal Immunol. *1*, 11–22.

Nair, N., Newell, E.W., Vollmers, C., Quake, S.R., Morton, J.M., Davis, M.M., He, X.S., and Greenberg, H.B. (2016). High-dimensional immune profiling of total and rotavirus VP6-specific intestinal and circulating B cells by mass cytometry. Mucosal Immunol. *9*, 68–82.

Narváez, C.F., Feng, N., Vásquez, C., Sen, A., Angel, J., Greenberg, H.B., and Franco, M.A. (2012). Human rotavirus-specific IgM Memory B cells have differential cloning efficiencies and switch capacities and play a role in antiviral immunity in vivo. J. Virol. *86*, 10829–10840.

Nutt, S.L., Hodgkin, P.D., Tarlinton, D.M., and Corcoran, L.M. (2015). The generation of antibody-secreting plasma cells. Nat. Rev. Immunol. *15*, 160–171.

Pape, K.A., Taylor, J.J., Maul, R.W., Gearhart, P.J., and Jenkins, M.K. (2011). Different B cell populations mediate early and late memory during an endogenous immune response. Science *331*, 1203–1207.

Petrof, E.O., Gloor, G.B., Vanner, S.J., Weese, S.J., Carter, D., Daigneault, M.C., Brown, E.M., Schroeter, K., and Allen-Vercoe, E. (2013). Stool substitute transplant therapy for the eradication of *Clostridium difficile* infection: 'RePOOPulating' the gut. Microbiome *1*, 3.

Planer, J.D., Peng, Y., Kau, A.L., Blanton, L.V., Ndao, I.M., Tarr, P.I., Warner, B.B., and Gordon, J.I. (2016). Development of the gut microbiota and mucosal IgA responses in twins and gnotobiotic mice. Nature *534*, 263–266.

Rubtsov, A.V., Rubtsova, K., Kappler, J.W., Jacobelli, J., Friedman, R.S., and Marrack, P. (2015). CD11c-expressing B cells are located at the T cell/B cell border in spleen and are potent APCs. J. Immunol. *195*, 71–79.

Seifert, M., Przekopowitz, M., Taudien, S., Lollies, A., Ronge, V., Drees, B., Lindemann, M., Hillen, U., Engler, H., Singer, B.B., and Küppers, R. (2015). Functional capacities of human IgM memory B cells in early inflammatory responses and secondary germinal center reactions. Proc. Natl. Acad. Sci. USA *112*, E546–E555.

Sintes, J., Romero, X., de Salort, J., Terhorst, C., and Engel, P. (2010). Mouse CD84 is a pan-leukocyte cell-surface molecule that modulates LPS-induced cytokine secretion by macrophages. J. Leukoc. Biol. *88*, 687–697.

Sohn, H.W., Krueger, P.D., Davis, R.S., and Pierce, S.K. (2011). FcRL4 acts as an adaptive to innate molecular switch dampening BCR signaling and enhancing TLR signaling. Blood *118*, 6332–6341.

Subramanian, A., Tamayo, P., Mootha, V.K., Mukherjee, S., Ebert, B.L., Gillette, M.A., Paulovich, A., Pomeroy, S.L., Golub, T.R., Lander, E.S., and Mesirov, J.P. (2005). Gene set enrichment analysis: a knowledge-based approach for interpreting genome-wide expression profiles. Proc. Natl. Acad. Sci. USA *102*, 15545–15550.

Tipton, C.M., Fucile, C.F., Darce, J., Chida, A., Ichikawa, T., Gregoretti, I., Schieferl, S., Hom, J., Jenks, S., Feldman, R.J., et al. (2015). Diversity, cellular origin and autoreactivity of antibody-secreting cell population expansions in acute systemic lupus erythematosus. Nat. Immunol. *16*, 755–765.

Tsuji, M., Suzuki, K., Kitamura, H., Maruya, M., Kinoshita, K., Ivanov, I.I., Itoh, K., Littman, D.R., and Fagarasan, S. (2008). Requirement for lymphoid tissue-inducer cells in isolated follicle formation and T cell-independent immunoglobulin A generation in the gut. Immunity *29*, 261–271.

van Zelm, M.C., Szczepanski, T., van der Burg, M., and van Dongen, J.J. (2007). Replication history of B lymphocytes reveals homeostatic proliferation and extensive antigen-induced B cell expansion. J. Exp. Med. *204*, 645–655.

Vander Heiden, J.A., Yaari, G., Uduman, M., Stern, J.N., O'Connor, K.C., Hafler, D.A., Vigneault, F., and Kleinstein, S.H. (2014). pRESTO: a toolkit for processing high-throughput sequencing raw reads of lymphocyte receptor repertoires. Bioinformatics *30*, 1930–1932.

Vossenkämper, A., Blair, P.A., Safinia, N., Fraser, L.D., Das, L., Sanders, T.J., Stagg, A.J., Sanderson, J.D., Taylor, K., Chang, F., et al. (2013). A role for gut-associated lymphoid tissue in shaping the human B cell repertoire. J. Exp. Med. *210*, 1665–1674.

Wang, N.S., McHeyzer-Williams, L.J., Okitsu, S.L., Burris, T.P., Reiner, S.L., and McHeyzer-Williams, M.G. (2012). Divergent transcriptional programming of class-specific B cell memory by T-bet and RORα. Nat. Immunol. *13*, 604–611.

Watanabe, K., Sugai, M., Nambu, Y., Osato, M., Hayashi, T., Kawaguchi, M., Komori, T., Ito, Y., and Shimizu, A. (2010). Requirement for Runx proteins in IgA class switching acting downstream of TGF-beta 1 and retinoic acid signaling. J. Immunol. *184*, 2785–2792.

Wettenhall, J.M., and Smyth, G.K. (2004). limmaGUI: a graphical user interface for linear modeling of microarray data. Bioinformatics *20*, 3705–3706.

Ye, J., Ma, N., Madden, T.L., and Ostell, J.M. (2013). IgBLAST: an immunoglobulin variable domain sequence analysis tool. Nucleic Acids Res. *41*, W34–W40.

Zuccarino-Catania, G.V., Sadanand, S., Weisel, F.J., Tomayko, M.M., Meng, H., Kleinstein, S.H., Good-Jacobson, K.L., and Shlomchik, M.J. (2014). CD80 and PD-L2 define functionally distinct memory B cell subsets that are independent of antibody isotype. Nat. Immunol. *15*, 631–637.

STAR★METHODS

KEY RESOURCES TABLE

REAGENT or RESOURCE	SOURCE	IDENTIFIER
Antibodies		
Rat anti human AID (clone: EK2 5G9)	Cell Signaling	4959S, RRID: AB_10692771
Anti-human CD1c PE (clone: L1S1)	Biolegend	331505, RRID: AB_1089000
Anti-human CD10 PE (clone: HI10a)	Biolegend	312203, RRID: AB_312203
Anti-human CD10 APC/Cy7 (clone: HI10a)	Biolegend	312212, RRID: AB_2146550
Anti-human CD11c PE (clone: B-ly6)	BD Biosciences	555392, RRID: AB_395793
Anti-human CD19 PE/Cy7 (clone: HIB19)	Biolegend	302215, RRID: AB_314245
Anti-human CD20 FITC (clone: 2H7)	BD Biosciences	555622, RRID: AB_395988
Anti-human CD21 PE(clone: B-ly4)	BD Biosciences	555422, RRID: AB_395816
Anti-human CD24 PE (clone: ML5)	BD Biosciences	555428, RRID: AB_395822
Anti-human CD27 PE (clone: O323)	eBioscience	12-0279-42, RRID: AB_10718394
Anti-human CD27 PerCP/Cy5.5 (clone: M-T271)	BD Biosciences	560612, RRID: AB_1727457
Anti-human CD35 PE (clone: E11)	Biolegend	333405, RRID: AB_2085021
Anti-human CD38 APC (clone: HIT2)	BD Biosciences	555462, RRID: AB_398599
Anti-human CD38 APC/Cy7 (clone: HIT2)	Biolegend	303534, RRID: AB_2561605
Anti-human CD43 PE (clone: 1G10)	BD Biosciences	560199, RRID: AB_1645655
Anti-human CD45 Alexa Fluor 700 (clone: HI30)	Biolegend	304024, RRID: AB_493761
Anti-human CD62L PE (clone: DREG-56)	Biolegend	304805, RRID: AB_314465
Anti-human CD66 a/c/e PE (clone: ASL-32)	Biolegend	342303, RRID: AB_1626288
Anti-human CD84 PE (clone: CD84.1.21)	Biolegend	326007, RRID: AB_2074766
Anti-human CD138 APC (clone: DL-101)	Biolegend	352307, RRID: AB_10901175
Anti-human CD138 PerCp/Cy5.5 (clone: DL-101)	Biolegend	352310, RRID: AB_10900979
Anti-human DEP-1/CD148 PE-conjugated (clone: 143-41)	R&D Systems	FAB1934P, RRID: AB_2174832
Anti-human CCR10 PE (clone: 6588-5)	Biolegend	341503, RRID: AB_1595542
Anti-human CCR7 PE (clone: G043H7)	Biolegend	353203, RRID: AB_10916391
Anti-human CCR9 PE (clone: L053E8)	Biolegend	358903, RRID: AB_2562384
Anti-human CXCR4 PE (clone: 12G5)	Biolegend	306505, RRID: AB_314611
Anti-human CXCR4 APC (clone: L291H4)	Biolegend	359407, RRID: AB_2562428
Anti-human FcRL4 APC (clone: 413D12)	Biolegend	340205, RRID: AB_10710013
Anti-human FcRL4 PE (clone: 413D12)	Biolegend	340203, RRID: AB_1575103
Anti-human HLA-DR Alexa Fluor 700 (clone: L243)	Biolegend	307626, RRID: AB_493771
Anti-human HLA-DR Brilliant Violet 605 (clone:L243)	Biolegend	307639, RRID: AB_11219187
Anti-human Ki-67 (clone: MIB-1)	DAKO	M7240, RRID: AB_2142367
Anti-human Ig light chain λ (clone: MHL-38)	Biolegend	316607, RRID: AB_493626
Anti-human IgA APC (clone: IS118E10)	Miltenyi Biotec	130-093-113, RRID: AB_1036152
Anti-human IgA-BIOT	Southern Biotech	2052-08
Anti-human IgA FITC (clone: IS118E10)	Invitrogen	H14101, RRID: AB_2536555
Anti-human IgA PE (clone: IS118E10)	Miltenyi Biotec	130-093-128, RRID: AB_1036158
FLEX Polyclonal Rabbit Anti-Human IgD Ready-to-Use	DAKO	IS517

(*Continued on next page*)

Continued

REAGENT or RESOURCE	SOURCE	IDENTIFIER
Anti-human IgD APC (clone: IA6-2)	BD Biosciences	561303, RRID: AB_10642578
Anti-human IgD PerCP/Cy5.5 (clone: IA6-2)	Biolegend	348208, RRID: AB_10641706
Anti-human IgD FITC	Southern Biotech	2032-02
Anti-human IgM Fc Secondary	Invitrogen	H15000, RRID: AB_2536556
Anti-human IgM APC (clone: SA-DA4)	Southern Biotech	9020-11
Anti-human IgM Brilliant Violet 605 (clone: MHM-88)	Biolegend	314523, RRID: AB_2562373
Anti-human/mouse Integrin β7 FITC (clone: FIB504)	Biolegend	321213, RRID: AB_830857
Anti-mouse IgD FITC (clone: 11-26c.2a)	BD Biosciences	558597, RRID: AB_647211
Anti-mouse CD45 PE/Cy7 (clone: 30-F11)	Biolegend	103113, RRID: AB_312978
Anti-mouse/human CD45R PE/Cy7 (clone: RA3-6B2)	Biolegend	103229, RRID: AB_492875
Anti-mouse CD138 Biotin (clone: 281-2)	Biolegend	142511, RRID: AB_2561980
Goat F(ab')2 Anti-Human IgA-PE	Southern Biotech	2052-09
Anti-mouse IgD Brilliant Violet 605 (clone: 11-26c.2a)	Biolegend	405727, RRID: AB_2562887
Anti-mouse IgM APC (clone: II/41)	BD	550676, RRID: AB_398464
Anti-mouse IgM FITC (clone: RMM-1)	Biolegend	466505, RRID: AB_315056
Anti-mouse IgA Secondary	Novus	NB7506, RRID: AB_10125106
Goat Anti-Mouse IgM-UNLB	Southern Biotech	1021-01
Goat Anti-Human Ig-UNLB	Southern Biotech	2010-01
Goat Anti-Human IgA-HRP	Southern Biotech	2050-05
Goat Anti-human IgM-HRP	Cappel	55255, RRID: AB_2334397
Bacterial and Virus Strains		
Escherichia coli	ATCC	25992
Bacillus cereus	ATCC	11778
Roseburia intestinalis	DSMZ	14610
Ruthenibacterium lactatiformans	DSMZ	100348
Bacteroides vulgatus	ATCC	8482
Bacteroides fragilis	ATCC	25285
Bacteroides thetaiotaomicron	ATCC	29148
Biological Samples		
Histologically normal tissue samples from terminal ileum and ascending colon	Patients undergoing right hemicolectomy-Hospital del Mar	N/A
Histological normal spleens	Hospital Clinic	N/A
Tonsils	Patients undergoing tonsillectomy-Hospital del Mar	N/A
Blood samples	BST-Barcelona	N/A
Chemicals, Peptides, and Recombinant Proteins		
4',6-Diamidine-2-phenylindole dihydrochloride (DAPI)	Sigma-Aldrich	28718-90-3
Ficoll-Paque PLUS	GE Healthcare	17144003
Collagenase IV	ThermoFischer	17104019
DNase	New England Biolab	M0303S
β-D-glucan from barley	Sigma	9041-22-9
Capsular polisaccharides (serotypes 9N, 14, 19F, 23F)	ATCC	N/A
Gal-α1,3-gal-HSA (3 atom spacer)	Dextra Laboratories	NGP2203
Laminarin from Laminaria digitata	Sigma-Aldrich	9008-22-4

(*Continued on next page*)

Continued

REAGENT or RESOURCE	SOURCE	IDENTIFIER
L-α-Phosphatidylcholine	Sigma-Aldrich	8002-43-5
megaCD40L	Enzo Life science	ALX-522-110-C010
TMB Substrate reagent set	BD bioscience	555214
IL-10	Peprotech	200-10
IL-21	Peprotech	200-21
CpG ODN-2006	ThermoFischer	tlrl-2006
BAFF (soluble)(human),(recombinant)	Enzo	ALX-522-025-C010
MEGACD40L (soluble)(human),(recombinant)	Enzo	ALX-522-110-C010
APRIL (human) (H98) (multimeric)	Adipogen	AG-40B-0088
FcR Blocking Reagent, human	Miltenyi	130-059-901
FluorSave reagent	Merck Millipore	345789
Syto BC	ThermoFischer	S34855
Critical Commercial Assays		
Giemsa Stain Kit (Jenner-Wright)	Agilent	AR308
CellTrace CFSE cell proliferation Kit	ThermoFisher	C34554
TaqMan Reverse Transcription Reagents	ThermoFisher	N8080234
Nextera XT DNA Sample Preparation Kits	Illumina	1502354
Pure Link Microbiome DNA Purification Kit	ThermoFisher	A29790
Quiamp DNA Mini Kit	QIAGEN	Cat# 51304
RNeasy Micro Kit	QIAGEN	Cat# 74004
AmpliTaq Gold PCR mastermix	ThermoFisher	4398881
Power SYBR Green PCR Master Mix	ThermoFisher	4367659
Deposited Data		
Microarray data	This Paper	GEO: GSE89282
NGS data	This Paper	BioProject: PRJNA355402
Experimental Models: Cell Lines		
EBV producing marmoset B cell line (B95-8)	ECACC	85011419
EBV transformed cell lines	This Paper	N/A
Oligonucleotides		
Primers for RT-PCR see Table S1	This paper	N/A
Primers for CSR see Table S2	This paper	N/A
Primers for NGS see Table S4	This paper	N/A
Software and Algorithms		
FlowJo v10.0.7	FlowJO	https://www.flowjo.com/
Fuji (ImageJ)	ImageJ	https://fiji.sc/
Gene Set Enrichment Analysis	(Subramanian et al., 2005)	http://software.broadinstitute.org/gsea/index.jsp
limmaGUI	(Wettenhall and Smyth, 2004)	https://www.bioconductor.org/packages/release/bioc/html/limmaGUI.html
pRESTO	(Vander Heiden et al., 2014)	https://presto.readthedocs.io
IgBLAST	(Ye et al., 2013)	https://www.ncbi.nlm.nih.gov/igblast/
Change-O	(Gupta et al., 2015)	https://changeo.readthedocs.io
R package	N/A	http://www.R-project.org/
IgTree Software	(Barak et al., 2008)	http://immsilico2.lnx.biu.ac.il/Software.html
QUIIME	(Caporaso et al., 2010)	http://qiime.org/
Prism v.6.0	GraphPad	www.graphpad.com
Ingenuity Pathway Analysis	QIAGEN	https://www.qiagenbioinformatics.com/

CONTACT FOR REAGENT AND RESOURCE SHARING

Further information and requests for resources and reagents should be directed to and will be fulfilled by the Lead Contact, Andrea Cerutti (acerutti@imim.es).

EXPERIMENTAL MODEL AND SUBJECT DETAILS

Human Tissue and Blood Specimens

Histologically normal tissue samples from terminal ileum and ascending colon were obtained from 50 patients undergoing right hemicolectomy due to colonic tumors, unresectable polyps or angiodysplasia. The age of these patients ranged from 28 to 89 years (mean 68.8 years) and the male/female ratio was 1:1.2. Peripheral mononuclear cells were isolated from buffy coats and splenocytes from histologically normal spleens from deceased organ donors or individuals undergoing post-traumatic splenectomy. Tonsils were obtained from adult patients with follicular hyperplasia. The use of blood and tissue samples was approved by the Ethical Committee for Clinical Investigation of the Institut Hospital del Mar d' Investigacions Mèdiques (CEIC-IMIM 2011/4494/I). Fresh tissue and mucus samples and formalin-fixed and paraffin-embedded tissue sections were collected from the Mar Biobanc tissue repository with patient-signed informed consent. All tissue samples were assigned coded identifiers and relevant clinical information remained concealed.

Mice

Female C57BL/6 mice (Charles River Laboratories) were bred in-house in the animal facility of the Barcelona Biomedical Research Park under specific pathogen free (SPF) or conventional housing conditions. All mice were used at 8-12 weeks of age. Mice were euthanized by cervical dislocation and animal procedures were approved by the Ethic Committee of the Barcelona Biomedical Research Park and performed according to Spanish and European legislations.

METHOD DETAILS

Sample Processing

For the isolation of mononuclear cells from human intestinal samples, mucosa and submucosa were dissected from muscularis externa and cut into 2-to-3-mm pieces. These pieces were first washed in calcium and magnesium-free Hanks' balanced salt solution (HBSS) before incubation at 37°C for 20 min in HBSS containing 5mM Dithiothreitol (DTT) and 1 mM Ethylenediaminetetraacetic acid (EDTA). The tissue pieces were transferred into a falcon tube with 30ml of HBSS and shaken vigorously for 10 s twice. The supernatant, containing the intra-epithelial lymphocytes fraction, was discarded. The remaining fraction was digested by incubation for 40 min at 37°C with stirring in a solution of HBSS containing 1 mg/ml collagenase IV (Thermo Fisher), 50ng/ml DNase (New England Biolabs) and 0.5% human serum (Sigma). Lamina propria (LP) suspensions were passed through a 70-μm filter, washed, and resuspended in RPMI 1640 medium (Thermo Fisher) with 10% fetal bovine serum (FBS). To isolate murine LP lymphocytes, upon excision of PPs, small intestine (SI) and large intestine (LI) segments were opened longitudinally and cut into 5-mm pieces. These pieces were subsequently processed following the same procedure used for human intestinal samples. Human splenocytes and tonsillar mononuclear cells were obtained from fresh samples by enzymatic digestion of the tissue for 40 min at 37°C in a solution of HBSS containing 1 mg/ml collagenase IV (Thermo Fisher), 50ng/ml DNase (New England Biolabs) and 0.5% human serum (Sigma), followed by separation on a Ficoll-Hypaque gradient (GE Healthcare). Peripheral blood mononuclear cells (PBMCs) were obtained from heparinized blood samples by separation on Ficoll-Hypaque gradient.

Flow Cytometry

Cells were incubated at 4°C with Fc-blocking reagent (Miltenyi Biotec) before the addition of the appropriate 'cocktails' of fluorochrome-labeled monoclonal antibodies (mAbs). Dead cells were excluded through the use of 4'-6'-diamidine-2′-phenylindole (DAPI) (Sigma). Cells were acquired with LSR Fortessa (BD Biosciences) and data were further analyzed with FlowJo V10 software (TreeStar).

Cell Sorting

For cell sorting, cell suspension were incubated at 4°C with Fc-blocking reagent (Miltenyi Biotec) and stained for 30min with the following monoclonal antibodies: anti-CD45 AF700 (clone: HI30), anti-CD19 PE-Cy7 (clone: HIB19), anti-CD38APC-Cy7 (clone: HIT2), anti-CD10 PE (clone: HI10a), anti-IgM BV605 (clone: MHM-88) (all from Biolegend), anti-CD27 PerCpCy5.5 (clone: M-T271) (BD Biosciences), and anti-IgD FITC (Southern). $CD45^+CD19^+CD38^{dull}CD10^-IgD^{2+}$ IgM^+CD27^- naive B cells, $CD45^+CD19^+CD38^{dull}$ $CD10^-IgD^+IgM^{2+}CD27^+$ MZ B cells, $CD45^+CD19^+CD38^{int}CD10^+$IgD-$IgM^+CD27^+$ GC-M, $CD45^+CD19^+CD38^{dull}CD10^-IgD^-IgM^+$ $CD27^+$ ME-M B cells, $CD45^+CD19^+$ $CD38^{dull}CD10^-$ $IgD^-IgM^-CD27^+$ ME-SW B cells, $CD45^+CD19^+CD38^{int}CD10^+IgD^-CD27^+$ GC B cells, $CD45^+CD19^+CD38^{2+}CD10^-IgD^-IgM^+CD27^+$ PC-M and $CD45^+CD19^+CD38^{2+}CD10^-$ $IgD^-IgM^+CD27^+$ switched PC were sorted with a FACSAria II (BD Biosciences) after exclusion of dead cells through DAPI staining. For sorting of $FCRL4^+$ and $FCRL4^-$ ME-M, anti-FCRL4 APC (clone: 413D12) was added to the 'cocktails'. The purity of cells sorted this way was consistently > 95%.

Cell Cultures

Human sorted intestinal naive and ME-M B cells (1 × 10^5/well) were seeded in 96-well U-bottomed plates (Thermo Fisher) and cultured for 6-7 days in complete RPMI 1640 medium (Thermo Fisher) supplemented with 10% FBS, penicillin and streptomycin (10 U/ml) with or without 200 ng/ml megaCD40L (Enzo Life Science), 50 ng/ml IL-10 (Peprotech), 500 ng/ml IL-21 (Peprotech), 1 μg/ml CpG ODN-2006 (Invivogen), 500 ng/ml BAFF (Alexis) and 100 ng/ml Mega APRIL (Alexis).

Proliferation Assay

Cell proliferation was assessed with carboxyfluorescein succinimidyl ester (CFSE) using CellTrace CFSE Cell Proliferation Kit (Thermo Fisher). Briefly, sorted lymphocytes were resuspended at 1x10^6 cell/ml in PBS supplemented with 5% FBS and incubated with 1.25μM CFSE solution for 5 min at room temperature (RT). Stained cells were extensively washed and cultured for 6-7 days in complete RPMI 1640 medium supplemented or not with specific stimuli. Cell division was assessed by measuring the decrease in CFSE fluorescence via flow cytometry.

Generation of EBV-Transformed B Cells

For the generation of EBV-transformed B cell lines, sorted B cells were seeded at 5 × 10^4 cells/well in 96 U-bottom plates (Thermo Fisher) in complete RPMI 1640 medium (Thermo Fisher) medium containing 2.5 μg/ml CpG ODN-2006 (Invivogen) and 30% supernatant from the EBV-producing marmoset B cell line B95-8 (ECACC). Proliferating cells were maintained in culture for 2-3 weeks and then frozen. Culture supernatants containing polyclonal immunoglobulins were stored at −80°C.

ELISA

Total and antigen-specific IgM and IgA from culture supernatants were detected by home-made ELISA. Briefly, 96 well ELISA plates (Thermo Fisher) were coated over night with goat anti-human Ig-UNLB (Southern Biotech) at 1ug/ml. To measure Ab-reactivity to specific antigens, ELISA plates were coated with either β-D-glucan (50 μg/ml; Sigma) or capsular polysaccharides (1 μg/ml; ATCC), Gal-α1,3-gal-HSA (3 atom spacer) (10 μg/ml; Dextra Laboratories), laminarin (50 μg/ml, Sigma) or L-α-Phosphatidylcholine (0.5 μg/ml; Bioresearch Technologies). For total Ig, serial dilutions of cell culture supernatants were added for 2 hr. for antigen-specific Ig, supernatants were used at 20 μg/ml Ig concentration and three 1:10 dilutions in PBS. All ELISAs were developed using HRP-labeled goat anti-human IgM (0.2 μg/ml; cappel) or IgA Fc Ab (0.25 μg/ml; Southern Biotech) and TMB substrate reagent set (BD Bioscience). OD450 was measured and Ab-reactivity was calculated after subtraction of background (OD450 of culture supernatants on PBS coated plates).

Immunofluorescence Analysis

Formalin-fixed paraffin-embedded human tissue sections 3-μm in thickness were treated in xylene, a decreasing alcohol gradient and distilled water to achieve de-waxing and rehydration of the tissue. Heat induced epitope retrieval was performed for 15 min in citrate buffer (pH 6) or Tris-EDTA buffer (pH 9). After epitope retrieval, tissue sections were permeabilized with 0.2% Triton X-100 in PBS, blocked with 5% bovine serum albumin and 5% Fc receptor blocking (Miltenyi Biotec) and stained with various combinations of antibodies to specific antigens. Biotinylated antibodies were detected with streptavidin–Alexa Fluor conjugates. Nuclear DNA was visualized with DAPI and coverslips applied with FluorSave reagent (Merck Millipore). Images were acquired either with a Leica TCS SP5 Upright confocal microscope (Leica) or a Nikon Eclipse Ni-E microscope (Nikon) and were further analyzed with ImageJ software.

Giemsa Staining

Cytospins were performed from sorted intestinal population at 800 rpm for 5 min using a Cytospin 4 apparatus (Thermo Fisher). Approximately 5,000 cells per subset were dried overnight on albumin-coated slides and stained with Giemsa Stain Kit (Jenner-Wright) (Agilent).

RNA Extraction and Reverse Transcription

Total cellular RNA was isolated with the RNeasy Micro kit (QIAGEN) by following the manufacturer's protocol. Approximately 2 ng of RNA with were reversed transcribed into cDNA using TaqMan® Reverse Transcription Reagents and Random hexamers (Thermo Fisher).

Quantitative Real Time and Standard PCR

Quantitative real time PCR (qRT-PCR) were performed in 384-well plates containing Power Sybr Green PCR Master Mix (Thermo Fisher) and specific primer pairs (**Table S1**) and analyzed on QuantStudio 12K Flex Real-Time PCR System (Thermo Fisher). Gene expression was normalized to that of the gene encoding β-actin (*ACTB*) for each sample and results were presented as relative expression (RE) compared to naive B cells. For the analysis of germline Iμ-Cμ, Iα-Cα1 and Iα-Cα_2 transcripts, PCRs were carried out using specific primers (**Table S2**) in a 50 μL PCR volume with AmpliTaq Gold PCR Mastermix (Thermo Fisher). Nested PCR analysis of Iα-Cμ circle transcript was carried out using two sets of specific primer pairs (**Table S2**) and the following cycling conditions. In the first PCR round, external primers were used in an initial denaturing step at 95°C for 9 min followed by 30 cycles comprised of 94°C for 30 s, 60°C for 1 min and 72°C for 10 min. In the second RT-PCR round, internal primers were used in an initial denaturing step at 95°C

for 9 min followed by 25 cycles comprised of 94°C for 30 s, 60°C for 1 min and 72°C for 10 min. PCR products were subjected to Sanger sequencing for confirmation.

KREC Assay

Genomic DNA was isolated from sorted B cell subsets with QIAamp DNA Mini Kit (QIAGEN). The replication history of B cell subsets was determined using the κ-deleting recombination excision circle (KREC) assay as described previously (van Zelm et al., 2007). This assay is based on a quantification of coding joints and signal joints of an Igκ-deleting rearrangement (intron RSS-Kde) by qRT-PCR. The ΔCT between the signal joint and the coding joint exactly represents the number of cell divisions a B cell has undergone. The previously established control cell line U698 DB01 (van Zelm et al., 2007) contains 1 coding and 1 signal joint per genome and was used to correct for minor differences in efficiency of both real-time quantitative-PCR assays.

Global Transcriptome Analysis

Total cellular RNA was isolated with the RNeasy Micro kit (QIAGEN) from sorted B cell subsets by following the manufacturer's protocol. RNA integrity was assessed using Agilent 2100 Bioanalyzer (Agilent). Only samples with high integrity (RNA integrity number $\geq$ 7) were used for transcriptome analysis. Amplification, labeling and hybridizations were performed according to protocol Ovation® Pico WTA System V2 and Encore Biotin Module (NuGEN) and then hybridized to GeneChip Human Gene 2.0 ST Array (Affymetrix) in a GeneChip Hybridization Oven 640. Washing and scanning were performed using the Expression Wash, Stain and Scan Kit (Affymetrix) and the Affymetrix GeneChip System including GeneChip Fluidics Station 450 and GeneChip Scanner 3000 7G. After quality control, raw data were background corrected, quantile-normalized and summarized to a gene-level using the robust multi-chip average (RMA) system. For the detection of differentially expressed genes, a linear model was fitted to the data and empirical Bayes moderated statistics were calculated using the *limma package* from Bioconductor (Wettenhall and Smyth, 2004). Adjustment of *p* values was performed by the determination of false discovery rates (FDR) using the Benjamini-Hochberg procedure. Genes with an adjusted *p* value less than 0.05 and with an absolute fold change value above 1.5 were selected as significant. Spearman's rank correlation was used to study correlation between normalized gene expressions of the different comparisons. Analyses were performed with R and standard packages. Comparison Upstream Regulator Analysis with Ingenuity Pathway Analysis (Ingenuity Systems, www.ingenuity.com) and GSEA from the Molecular Signature Database (MSigDB) (Subramanian et al., 2005) were used to identify similarities and differences among samples.

Next Generation Sequencing of Ig Gene Repertoires

Aliquots of cDNA products from sorted B cells (**Table S3**) were mixed with high performance liquid chromatography-purified primers specific for VH1-VH6 framework region 1 (50 nM) and primers specific for Cα or Cμ (250 nM) containing corresponding Illumina Nextera sequencing tags (**Table S4**) in a PCR volume of 25 μL (4 μL template cDNA) with High Fidelity Platinum PCR Supermix (Thermo Fisher). Amplification was performed using the following conditions. An initial step of 95°C for 5 min was followed by 35 cycles including 95°C for 30 s, 58°C for 30 s, and 72°C for 30 s, supplemented with a final extension step of 72°C for 5 min. Products were purified with miniElute PCR purification Kit (QIAGEN) and Nextera indices were added via PCR with the following conditions: 72°C for 3 min, 98°C for 30 s, 5 cycles of 98°C for 10 s, 63°C for 30 s, and 72°C for 3 min. Ampure XP beads (Beckman Coulter Genomics) were used for purification of the PCR products, which were subsequently pooled and denatured. Single-strand products were paired-end sequenced on a MiSeq (Illumina) with the 500 Cycle v2 Kit (2 × 250 bp). In total, 4,898,226 IGHV gene sequences from four donors were obtained through next generation sequencing (**Table S3**). Paired-end raw sequencing reads were processed into donor-specific Ig gene sequences and grouped in clonal families using a bioinformatics pipeline based on pRESTO, IgBLAST and Change-O (Gupta et al., 2015; Vander Heiden et al., 2014; Ye et al., 2013). First, raw reads with a Phred score lower than 20 were filtered out, and primers for CH and VH genes were masked. Next, corresponding paired-end reads were aligned and merged together (minimum overlap of 6 nucleotides) and annotated with donor, cell type and isotype origin. Finally, donor-specific Ig subsets were combined (prior to VDJ annotation) to estimate donor-specific clonal families. VDJ calling and assignment were performed using the default parameters for IgBLAST and querying the latest downloaded human IGH IMGT database from February 2016. Donor-specific clonal groups were inferred using a distance-based clustering method implemented in Change-O. Sequences with the same VH and JH annotation, identical H-CDR3 region length and Hamming distance higher than 85% were considered to belong to the same clonal group or family. Finally, germline sequences for each clone were reconstructed using the annotated VDJ information as implemented in Change-O. Donor-specific clonal groups were represented through RCircos plots to visualize the relationships between B cell subsets at clonal level. Morisita-Horn Index estimates were calculated using the *divo* R package. In both analyses, a rarefied sample of 10,000 clones per subset was used to account for possible sample size biases between donors, tissues and cell types. MHI bootstrap estimates were calculated by resampling 1,000 times a subsample of 10,000 clones for each tissue, cell type and donor. VH and JH gene usage was estimated for each donor and B cell subset, with bars representing average values among donors. SHM levels were estimated by averaging the number of mutations compared to the inferred germline sequence of each clone belonging to a given B cell subset and donor. Donor-specific clonally related B cell lineage trees were reconstructed and plotted using IgTree Software (Barak et al., 2008).

Mucus Collection and Processing

Mucus was obtained by scrapping off the epithelial surface of macroscopically unaffected fresh tissue samples from terminal ileum and ascending colon of patients undergoing right hemicolectomy. Intestinal contents from murine SI and LI segments were removed by running forceps along a given intestinal segment and placed in a 1.5 mL Eppendorf tube on ice. Aliquots of microbial samples from mucus or intestinal contents were weighed and resuspended at 0.1 mg/μL in PBS with protease inhibitors from SIGMAFAST Protease Inhibitor Tablets (Sigma). Samples were homogenized by vigorously vortexing for 5 min and then centrifuged at 400 g for 5 min to pellet large debris. The supernatant was filtered through a sterile 70 μm cell strainer and centrifuged at 8000 g for 5 min to pellet microbes. At this stage, supernatants were saved and frozen at −80°C for the analysis of free SIgM and Sig and microbial pellets were used for bacterial flow cytometry and FACSorting.

Bacterial Flow Cytometry and FACSorting

To measure endogenous SIgM and SIgA bound to intestinal bacteria, microbial pellets were resuspended in PBS 5% FBS and incubated for 30 min on ice with the following combination of antibodies: anti-human IgM APC (clone: SA-DA4) (Southern Biotech) and anti-human IgA PE (Miltenyi Biotec). Finally, bacterial samples were washed and resuspended in PBS with SYTO BC (Thermo Fisher) for 15 min on ice to perform FCM analysis. To measure reactivity of IgM from EBV-transformed B cells against intestinal microbiota, endogenous bacteria-bound SIgs were stripped following incubation for 3 min in an acidic sodium citrate buffer (40 mM sodium citrate and 140 mM NaCl, pH 3.0). Then, microbes were quickly spun down to remove the buffer and PBS was added for pH neutralization. These samples were incubated with supernatants from EBV-transformed B cells (at 50 μg/ml total IgM) for 30 min on ice. After washing, microbial pellets were resuspended in MACS 5% FBS and incubated for 30 min on ice with anti-human IgM APC (clone: SA-DA4) (Southern Biotech). Finally, samples were washed and resuspended in PBS with SYTO BC (Thermo Fisher) for 15 min on ice for FCM analysis. To measure reactivity of IgM from EBV-transformed B cells against specific bacterial species (*Escherichia coli, Bacillus cereus, Bacteroides vulgatus, Bacteroides fragilis*, *Bacteroides thetaiotaomicron*-all from ATCC and *Ruthenibacterium lactatiformans* and *Roseburia intestinalis* from DSMZ), 10^5 to 10^6 heat inactivated bacteria (65°C for 20 min) were incubated for 15 min at RT with graded amounts of IgM from EBV-transformed ME-M B cell lines (from 0.18 to 15 μg/ml total IgM). After washing, microbial pellets were resuspended in PBS and incubated for 15min with anti-human IgM APC (clone: SA-DA4) (Southern Biotech) in the presence of SYTO BC (Thermo Fisher). Contamination was minimized by passing all buffers and media through sterile 0.22-μm filters before use. In all settings, bacterial FCM was performed using a FORTESSA Cytometer (BD Bioscience) with low forward scatter (FSC) and side scatter (SSC) thresholds to allow bacterial detection. FSC and SSC were set to a Log scale and samples were gated $FSC^+SSC^+SYTO\ BC^+$ and then assessed for IgA and IgM staining. Microbial samples were sorted using a FACSAria II (BD Biosciences) instrument. Threshold settings were set to the minimal allowable voltage for SSC and 50,000 events were collected from $SIgA^-SIgM^-$, $SIgA^+SIgM^-$ or $SIgA^+SIgM^+$ fractions gates as shown in Figure 7A. Each fraction (typically 50 μL) was stored at −20°C before performing PCR and sequencing of bacterial 16S rRNA genes. Multiple precautions were taken to minimize potential contamination of FACSorted fractions, including collecting samples from the flow cytometer droplet stream (sheath fluid) immediately before each sorting to allow assessment of any potential contaminants in fluid lines.

Bacterial 16S rRNA Gene Analysis

DNA was extracted from unsorted mucus samples using PureLink Microbiome DNA Purification Kit (Thermo Fisher) following the manufacturer's instructions and amplicons of V3-V4 regions of 16S rRNA genes were generated as described below. 16S rRNA amplicons from FACSorted bacteria were generated by adding 2.5 μL of each bacterial fraction directly to Platinum® PCR SuperMix High Fidelity (Thermo Fisher) containing PCR primers that target 16S V3 and V4 region (**Table S4**) in triplicate 20cμl reactions. 16S rRNA analysis was performed on samples collected from the flow cytometer droplet stream before every sort (sheath fluid), which permitted the identification of sequences that did not originate from the sorted sample. The following PCR conditions were used: an initial denaturation step at 95c°C for 10cmin was followed by 35 cycles that included 95c°C for 30csec, 55c°C for 30csec, and 72°C for 30 s, with an ending step of 72c°C for 5cmin. Triplicate reactions were pooled and subjected to 1% agarose gel electrophoresis to verify the presence of a PCR product (these gels also contained negative control reactions). Pooled amplicons were purified with AMPure XP magnetic beads (Agencourt) and subjected to multiplexed sequencing (paired-end 250 nucleotide reads) on a MiSeq instrument (Illumina) with the 500 Cycle V2 Kit (2 × 250 bp). Paired-end reads were filtered (Phred > 19) and merged using the *fastq-join* algorithm. De-multiplexed reads were clustered into operational taxonomic units (OTUs) with a 97% identity sequence using the gg_13_5 release from Greengenes database as well as the default open reference QUIIME pipeline for Ilumina reads (Caporaso et al., 2010). Similar to FACSorted fractions, sheath fluid samples were sequenced and processed to identify putative contaminant OTUs. A comparison against ''high-biomass'' samples (mucus) was performed to pick the most frequent contaminant OTU found in the sheath fluid but not in ''high-biomass'' samples. This reference contaminant OTU was then used to proportionally remove all the other contaminant OTUs found in either sheath fluid or FACSorted samples. Finally, an 'abundance-filtered dataset' was generated by selecting OTUs that were detected at > 0.1% relative abundance in each sample. This OTU table was then rarefied to the minimum sample's depth (27529 reads). Rarefied alpha diversity plots for Shannon Index and Phylogenetic Diversity (PD_whole_tree) were generated using default QIIME scripts. A log-transformed Enrichment Index (EI) was calculated for each OTU and sample according to the formula shown in Figure 7F. Only OTUs present in input samples at least 3 times and at a frequency higher than 0.1% were used to build the final EI distributions. The heatmap plot was generated using mean values from EI distributions. OTUs and fractions were then grouped through a hierarchical clustering algorithm.

Quantification and Statistical Analysis

Differences between means from independent groups were assessed using Prism 5.03 software (GraphPad) and R studio. For comparison of two groups, *P* values were determined by unpaired two-tailed Student's t test, unless otherwise indicated. For comparison of more than two groups, significant values were calculates via one-way ANOVA with Tukey's post hoc test. p values < 0.05 were considered significant. P values are indicated on plots and in figure legends. (* $p < 0.05$, ** $p < 0.01$, *** $p < 0.001$).

DATA AND SOFTWARE AVAILABILITY

The Gene Expression Omnibus accession number for the global gene transcriptional analysis reported in this paper is GEO: GSE89282. Sequencing data are publicly available under BioProject accession number BioProject: PRJNA355402.